



# HHS Public Access

## Author manuscript

*Nat Genet.* Author manuscript; available in PMC 2018 April 30.

Published in final edited form as:

*Nat Genet.* 2017 December ; 49(12): 1779–1784. doi:10.1038/ng.3984.

## Computational correction of copy-number effect improves specificity of CRISPR-Cas9 essentiality screens in cancer cells

Robin M. Meyers<sup>1,†</sup>, Jordan G. Bryan<sup>1,†</sup>, James M. McFarland<sup>1</sup>, Barbara A. Weir<sup>1</sup>, Ann E. Sizemore<sup>1</sup>, Han Xu<sup>1</sup>, Neekesh V. Dharia<sup>1,2,3,4</sup>, Phillip G. Montgomery<sup>1</sup>, Glenn S. Cowley<sup>1</sup>, Sasha Pantel<sup>1</sup>, Amy Goodale<sup>1</sup>, Yenarae Lee<sup>1</sup>, Levi D. Ali<sup>1</sup>, Guozhi Jiang<sup>1</sup>, Rakela Lubonja<sup>1</sup>, William F. Harrington<sup>1</sup>, Matthew Strickland<sup>1</sup>, Ting Wu<sup>1</sup>, Derek C. Hawes<sup>1</sup>, Victor A. Zhivich<sup>1</sup>, Meghan R. Wyatt<sup>1</sup>, Zohra Kalani<sup>1</sup>, Jaime J. Chang<sup>1</sup>, Michael Okamoto<sup>1</sup>, Kimberly Stegmaier<sup>1,2,3,4</sup>, Todd R. Golub<sup>1,2,3,4,5</sup>, Jesse S. Boehm<sup>1</sup>, Francisca Vazquez<sup>1,2</sup>, David E. Root<sup>1</sup>, William C. Hahn<sup>1,2,4,6,\*</sup>, and Aviad Tsherniak<sup>1,\*</sup>

<sup>1</sup>Broad Institute of MIT and Harvard, 415 Main Street, Cambridge, MA 02142 USA

<sup>2</sup>Dana-Farber Cancer Institute, 450 Brookline Avenue, Boston, MA 02215 USA

<sup>3</sup>Boston Children's Hospital, 300 Longwood Avenue, Boston, MA 02215 USA

<sup>4</sup>Harvard Medical School, 25 Shattuck Street, Boston, MA 02115 USA

<sup>5</sup>Howard Hughes Medical Institute, 4000 Jones Bridge Road, Chevy Chase, MD 20815 USA

<sup>6</sup>Department of Medicine, Brigham and Women's Hospital, 75 Francis Street, Boston, MA 02115

### Abstract

The CRISPR-Cas9 system has revolutionized gene editing both on single genes and in multiplexed loss-of-function screens, enabling precise genome-scale identification of genes essential to proliferation and survival of cancer cells<sup>1,2</sup>. However, previous studies reported that a gene-

---

Users may view, print, copy, and download text and data-mine the content in such documents, for the purposes of academic research, subject always to the full Conditions of use: [http://www.nature.com/authors/editorial\\_policies/license.html#terms](http://www.nature.com/authors/editorial_policies/license.html#terms)

\*Corresponding authors: aviad@broadinstitute.org, william\_hahn@dfci.harvard.edu.

†These authors contributed equally

### Materials and correspondence

Correspondence or requests for materials should be addressed to either Aviad Tsherniak (aviad@broadinstitute.org) or William C. Hahn (william\_hahn@dfci.harvard.edu).

### Code availability

We have made the CERES software and documentation available as an R package at <https://depmap.org/ceres>. We have deposited a code repository of scripts for regenerating analyses and figures here as well.

### Data availability

We have made all CRISPR-Cas9 screening data presented here available at <https://depmap.org/ceres>. We also have posted these data and all other datasets used for analysis in a Figshare record, available at <https://doi.org/10.6084/m9.figshare.5319388>.

### Author contributions

R.M.M., J.G.B., and A.T. conceived of and designed the study. R.M.M., J.G.B., and J.M.M. performed computational analysis and interpretation of results. J.G.B. wrote and implemented the modeling software. R.M.M., B.A.W., and A.E.S. processed and managed data. H.X., and N.V.D. assisted with computational analysis. P.G.M. provided computational tools. G.S.C., S.P., and F.V. provided project management. A.G., Y.L., L.D.A., G.J., R.L., W.F.H., M.S., T.W., D.C.H., V.A.Z., M.R.W., Z.K., J.J.C., and M.O. assisted with data generation. R.M.M., J.G.B., J.M.M., W.C.H., and A.T. wrote and/or revised the manuscript with assistance from other authors. K.S., T.R.G., J.S.B., F.V., D.E.R., W.C.H., and A.T. supervised the study and performed an advisory role.

### Competing financial interests

W.C. Hahn reports receiving a commercial research grant from Novartis and is a consultant/advisory board member for the same as well as for KSQ Therapeutics. No potential conflicts of interest were disclosed by the other authors.

Author Manuscript  
Author Manuscript  
Author Manuscript  
Author Manuscript

independent anti-proliferative effect of Cas9-mediated DNA cleavage confounds such measurement of genetic dependency, leading to false positive results in copy number amplified regions<sup>3,4</sup>. We developed CERES, a computational method to estimate gene dependency levels from CRISPR-Cas9 essentiality screens while accounting for the copy-number-specific effect. As part of our efforts to define a cancer dependency map, we performed genome-scale CRISPR-Cas9 essentiality screens across 342 cancer cell lines and applied CERES to this dataset. We found that CERES reduced false positive results and estimated sgRNA activity for both this dataset and previously published screens performed with different sgRNA libraries. Here, we demonstrate the utility of this collection of screens, upon CERES correction, in revealing cancer-type-specific vulnerabilities.

---

Significant efforts using loss-of-function genetic screens to systematically identify genes essential to the proliferation and survival of cancer cells have been reported<sup>1-10</sup>. Genes identified by these approaches may represent specific genetic vulnerabilities of cancer cells, suggesting treatment strategies and directing the development of novel therapeutics. The CRISPR-Cas9 genome editing system has proven to be a powerful tool for multiplexed screening due to its relative ease of application and increased specificity compared to RNA interference technology<sup>11</sup>.

However, we and others have recently observed that measurements of cell proliferation in genome-scale CRISPR-Cas9 loss-of-function screens are influenced by the genomic copy number (CN) of the region targeted by the sgRNA-Cas9 complex<sup>1,3,4</sup>. Targeting Cas9 to DNA sequences within regions of high CN gain creates multiple DNA double-strand breaks (DSBs), inducing a gene-independent DNA damage response and a G2 cell-cycle arrest phenotype<sup>3</sup>. This systematic, sequence-independent effect due to DNA cleavage (*copy-number effect*) confounds the measurement of the consequences of gene deletion on cell viability (*gene-knockout effect*) and is detectable even among low-level CN amplifications and deletions. In particular, this phenomenon hinders interpretation of experiments performed in cancer cell lines that harbor many genomic amplifications since genes in these regions represent a major source of false positives<sup>3,4</sup>. Existing methods to handle the copy-number effect adopt filtering schemes<sup>9</sup>, which preclude examination of data from within amplified regions and ignore the effect at low-level alterations. Here, we present CERES, a method to estimate gene dependency from essentiality screens while computationally correcting the copy-number effect, enabling unbiased interpretation of gene dependency at all levels of CN.

As part of our efforts to define a Cancer Dependency Map, a catalog of cell line-specific genetic and chemical vulnerabilities<sup>10,12</sup>, we performed genome-scale CRISPR-Cas9 loss-of-function screens in 342 cancer cell lines representing 27 cell lineages (Supplementary Table 1, <http://depmap.org/ceres>) using the Avana sgRNA library<sup>13</sup> (Supplementary Table 2) and assessed the effects of introducing each sgRNA on cell proliferation (Online Methods). After applying quality control measures, ROC analysis of sgRNAs targeting “gold standard” common core essential and nonessential genes<sup>14</sup> demonstrated high screen quality in all cell lines (Fig. 1a). This collection of screens surpasses the scale of existing comparable datasets by roughly tenfold. To confirm the generalizability of our results in independent screens

performed with different sgRNA libraries, we reanalyzed two published datasets derived from screens across 33 cancer cell lines of diverse cell lineage (GeCKOv2)<sup>3</sup> and 14 AML cell lines (Wang2017)<sup>9</sup> (Supplementary Fig. 1a).

Using genomic copy number data from the Cancer Cell Line Encyclopedia (CCLE)<sup>15</sup>, we assessed the 342 cell lines screened in our Avana dataset for sensitivity to the copy-number effect as in Aguirre *et al.*<sup>3</sup>. In consonance with previous observations, the relationship held in every cell line in our panel, where sgRNAs targeting more genomic loci were on average more depleted, frequently to levels at or below the depletion of sgRNAs targeting cell-essential genes (Fig. 1b, Supplementary Fig. 1b,c). In each of the three datasets, some of the observed variability in sensitivity was explained by the p53 mutational status of each line in CCLE (Supplementary Fig. 1d).

To quantify the extent to which this sgRNA-level effect translates into false positive gene dependencies, we ranked the genes in each cell line by the average depletion of their targeting sgRNAs (*average guide score*). In an example breast cancer cell line, HCC1419, high-ranking genes were enriched for both genes involved in fundamental cellular processes and genes with amplified CN (Fig. 1c). The depletion ranks of the 100 genes with the largest CN measurements were significantly higher than expected for the majority of cell lines (298/342 with  $p < 0.05$ , one-sample one-tailed K-S test; Fig. 1d, Supplementary Fig. 2a) and the extent of enrichment was significantly correlated with the average CN of these genes (Spearman  $\rho = 0.61$ ,  $p < 10^{-15}$ ), consistent with previous studies (Supplementary Fig. 2b).

To decouple the gene-knockout effect from the copy-number effect, we developed CERES, which computationally models the measured sgRNA depletion ( $D$ ) as a sum of these two effects (Fig. 2, Online Methods). Specifically, for each sgRNA  $i$  and cell line  $j$ , CERES assumes the following model (**Equation 1**):

$$D_{ij} = q_i \left( \sum_{k \in G_i} (h_k + g_{kj}) + f_j \left( \sum_{l \in L_i} C_{lj} \right) \right) + o_i + \varepsilon$$

where  $\varepsilon$  is a zero-mean, independent Gaussian noise term. The gene-knockout effect is a sum of cell line specific ( $g_{kj}$ ) and shared ( $h_k$ ) effects, which are aggregated across any gene targeted by sgRNA  $i$  ( $G_i$ ). The copy-number effect is modeled by a piecewise linear spline,  $f_j$ , evaluated at the number of genomic sites targeted, determined by the target loci ( $L_i$ ) and the CN at each locus ( $C_{lj}$ ) (Online Methods). The cumulative depletion effects are then scaled by a *guide activity score* ( $q_i$ ), restricted to values between 0 and 1, to capture and mitigate the influence of low-quality reagents<sup>13,16,17</sup>. The offset term  $o_i$  accounts for noise in the measurement of sgRNA abundance in the reference pool (Online Methods). CERES infers the gene-knockout effects and all other parameters by fitting the model to the observed data via alternating least squares regression (Online Methods). The inferred gene-knockout effects are then scaled per cell line such that scores of 0 and -1 represent the median effects of nonessential genes and common core essential genes, respectively.

We applied CERES to the Avana dataset of 342 essentiality screens, as well as the GeCKOv2 and Wang2017 datasets, and analyzed the inferred gene-knockout effects (Supplementary Tables 3–5). As expected, CERES markedly reduced the relationship between CN and gene dependency found in the uncorrected average guide scores (Fig. 3a, Supplementary Fig. 3a) and removed it nearly entirely among unexpressed genes, determined using CCLE expression data (Supplementary Fig. 3b). For each gene, we correlated its CN measurements to its dependency scores before and after correction and found that CERES shifted the mean correlation to near zero (Supplementary Fig. 3c). CERES also improved the identification of essential genes in 339 out of 342 screens, as measured by the recall of common core essential genes at a 5% false discovery rate (FDR) of nonessential genes<sup>2</sup>, by an average of 13.8 percentage points (Fig. 3b, Supplementary Fig. 4a) (Online Methods). This improvement was substantially better than a simple linear model used to correct the relationship between average guide score and CN (Supplementary Fig. 4b) (Online Methods). Furthermore, CERES preserved an average of 134 genes per cell line that would have been removed using a simple filtering scheme. On average, six of these filtered genes per cell line scored as essential below a threshold of  $-0.6$  after CERES correction (Supplementary Fig. 4c). Reassuringly, CERES preserved expected cancer-specific dependencies, even in amplified regions, such as *KRAS* in an example amplification on chromosome 12p of the DAN-G pancreatic cancer cell line (Fig. 3c, Supplementary Fig. 5). Additionally, *KRAS*-mutant cell lines remained substantially enriched over wild-type for *KRAS* gene dependency (Fig. 3d), which generalized to other known oncogenes (Supplementary Fig. 6).

CERES estimates a guide activity score for each sgRNA used in the screens (Supplementary Tables 6–8). While it is infeasible to experimentally validate the activity of all, or even most, sgRNAs in a genome-scale library, sequence determinants have proven useful in the prediction of on-target activity<sup>13,18,19</sup>. The Avana sgRNA library was optimized using such predictions. Fittingly, CERES estimated higher guide activity scores on average for the Avana dataset relative to GeCKOv2, with a nearly twenty-fold increase in the ratio of high-to low-activity sgRNAs (161.3 to 1 and 8.3 to 1; Fig. 4a). The guide activity scores for the 4,770 sgRNAs common to both libraries showed substantial agreement (Spearman  $\rho = 0.53$ ,  $p < 10^{-15}$ ; Fig. 4b), demonstrating that CERES captured a measure of sgRNA activity that is reproducible across independent collections of screens (Supplementary Fig. 7a,b). For both the GeCKOv2 and Avana libraries, we compared CERES guide activity scores to sequence-based predictions of sgRNA activity (Doench-Root scores)<sup>13</sup> and found significant correspondence (Avana: Pearson  $\rho = 0.21$ ,  $p < 10^{-15}$ ; GeCKOv2: Pearson  $\rho = 0.37$ ,  $p < 10^{-15}$ ; Fig. 4c). Taken together, these results demonstrate that the guide activity scores inferred by CERES are useful for estimating gene-knockout effects and, furthermore, suggests that they could assist in the selection of reagents for follow-up experiments.

To identify cancer-specific genetic vulnerabilities, we used a metric of differential dependency representing the strength of dependency in a cell line relative to all other lines screened (Online Methods). We assessed an upper bound on the number of false positive differential dependencies due to CN amplifications by calculating the percentage of amplified genes at every possible threshold of differential dependency. In the uncorrected data, the percentage of amplified genes increased at stronger dependency thresholds,

climbing above 30% at the highest levels of differential dependency, which CERES substantially reduces (Fig. 5a, Supplementary Fig. 8a). We next used a similar procedure to examine unexpressed genes, whose deletion or editing is not expected to induce phenotypic effects, and which represent an overt source of false positives if scored as differentially dependent. We found that for genes below a differential dependency of -8, CERES reduced the percentage of unexpressed genes from 6.6% to 0.9%, indicating a substantial improvement in specificity (Fig. 5b, Supplementary Fig. 8b).

A dataset of this scale enables the discovery of genetic vulnerabilities specific to a subset of cancer cell lines defined by some cellular context, such as cell lineage. We hypothesized that in this setting, copy-number effects driven by recurrent CN alterations, even with small effect sizes, could introduce false positives. For each gene, we compared average guide scores in 26 breast cancer cell lines to those of all other cell lines (Online methods). Indeed, we found several differential dependencies resident on chromosome 8q, which is recurrently amplified in breast tumors (Fig. 6a). However, when we used CERES-corrected dependency scores, we found that only two of the original chr8q genes, *TRPS1* and *GRHL2*, remained (Fig. 6b). To confirm this finding using a complementary assay, we analyzed this set of genes in a dataset derived from genome-scale RNAi screens across 501 cancer cell lines<sup>20</sup>. We found that these were the only two genes on chr8q that scored as differentially dependent in the 34 breast lines, while most genes in other regions validated (Supplementary Fig. 9a,b). Previous studies have implicated these transcription factors in breast cancer progression<sup>21,22</sup>, and the high expression levels of these and other transcription factors in breast lines identified suggest that they are likely to be true differential dependencies (Supplementary Fig. 9c). We extended this analysis to all cell lineages with recurrently amplified chromosome arms and quantified the enrichment of differential dependencies before and after CERES correction in each context. We observed that CERES reduced the fraction of differential dependencies on the recurrently amplified chromosome arm in 24 out of 25 such cases (Fig. 6c) (Online Methods).

While CERES leverages data across many cell lines to infer guide activity scores, we confirmed that this approach can be applied to datasets of any size - even a screen of a single cell line - given predetermined guide activity scores. These may be pre-computed from a larger set of screens, predicted using available tools, or assumed uniform. In random subsamplings of cell lines from the Avana dataset, CERES performed nearly as well as when applied to the full set. Furthermore, we tested CERES on single cell lines, using fixed uniform guide activities, and found that the median improvement per cell line was over 97% that of the run on all 342 cell lines (Supplementary Fig 10) (Online Methods).

In summary, we introduce a large set of uniformly performed CRISPR-Cas9 essentiality screens of cancer cell lines, propose a methodology to estimate gene dependency while removing false positives due to copy-number effects, and demonstrate the power of these two resources in revealing genetic vulnerabilities of cancer. To facilitate the use of the Avana dataset and CERES, we make the software available as an R package at <https://depmap.org/ceres>, along with all data and analysis scripts used in this study.

## Online Methods

### CRISPR-Cas9 essentiality screening assay

Cancer cell lines were transduced with a lentiviral vector expressing the Cas9 nuclease under blasticidin selection (pXPR-311Cas9). Each Cas9-expressing cell line was subjected to a Cas9 activity assay<sup>3</sup> to characterize the efficacy of CRISPR/Cas9 in these cell lines (Supplementary Table 1). Cell lines with less than 45% measured Cas9 activity were considered ineligible for screening. Stable polyclonal Cas9+ cell lines were then infected in replicate ( $n = 3$ ) at low multiplicity of infection (MOI < 1) with a library of 76,106 unique sgRNAs (Avana), which after filtering out sex chromosomes was composed of 70,086 targeting 17,670 genes (~4 sgRNAs per gene) annotated in the consensus coding sequence (CCDS) database, and 995 non-targeting control sgRNAs (Supplementary Table 2). Cells were selected in puromycin and blasticidin for 7 days and then passaged without selection while maintaining a representation of 500 cells per sgRNA until 21 days after infection. Genomic DNA was purified from endpoint cell pellets, the sgRNA barcodes are PCR amplified with sufficient gDNA to maintain representation, and the PCR products are sequenced using standard Illumina machines and protocols.

### Preprocessing and quality control

After sequencing the sgRNA barcodes, raw barcode counts are deconvoluted from sequence data using PoolQ software ([http://portals.broadinstitute.org/gpp/public/dir/download?dirpath=protocols/screening&filename=Pooled\\_Screening\\_Deconvolution\\_using\\_PoolQ.pdf](http://portals.broadinstitute.org/gpp/public/dir/download?dirpath=protocols/screening&filename=Pooled_Screening_Deconvolution_using_PoolQ.pdf)) and are summed across sequencing lanes. Samples were removed if they failed to reach 15 million reads. We calculated normalized read counts for each sample according to the procedure in Cowley et al.<sup>7</sup>. We then calculated pairwise Pearson correlation coefficients between replicate samples from the same cell line to identify and remove poor quality replicates using a threshold of 0.7. All sample read counts were then divided by their representation in the starting plasmid DNA library (pDNA) to compute a fold-change (FC). We computed robust Strictly Standardized Mean Difference (SSMD)<sup>23</sup> statistics for the replicates using FCs between non-targeting control sgRNAs and FCs from sgRNAs targeting the spliceosomal, ribosomal, or proteasomal genes in KEGG genesets<sup>24–26</sup>. We remove replicates with SSMDs that fail to reach -0.5. We also followed standard fingerprinting procedures to remove mismatched cell lines<sup>7</sup>. logFC data were then normalized within each cell line replicate by subtracting the median logFC value and dividing by the median average deviation (MAD) before input to CERES.

### Copy number data

Copy number data for all cancer cell lines were obtained from the Cancer Cell Line Encyclopedia (CCLE)<sup>15</sup> data portal (<https://portals.broadinstitute.org/ccle>). CN data were derived from Affymetrix SNP6.0 arrays. Segmentation of normalized log2 ratios was performed using the circular binary segmentation (CBS) algorithm. The dataset is available at ([https://data.broadinstitute.org/ccle\\_legacy\\_data/dna\\_copy\\_number/CCLE\\_copynumber\\_2013-12-03.seg.txt](https://data.broadinstitute.org/ccle_legacy_data/dna_copy_number/CCLE_copynumber_2013-12-03.seg.txt)).

## Gene expression and mutation data

Gene expression and mutation data for all cell lines were obtained from CCLE data portal. These datasets are available at [https://data.broadinstitute.org/cCLE/CCLE\\_RNAseq\\_081117.rpkpm.gct](https://data.broadinstitute.org/cCLE/CCLE_RNAseq_081117.rpkpm.gct) and [https://data.broadinstitute.org/cCLE/cCLE2maf\\_081117.txt](https://data.broadinstitute.org/cCLE/cCLE2maf_081117.txt).

## sgRNA genome mapping

sgRNA sequences are mapped to the *hg19* reference genome using the bowtie short read aligner, version 1.1.2<sup>27</sup>. Bowtie was run using the options “-a -v 0” in order to find all perfect matches in the genome. Only sgRNAs with fewer than 100 alignments were included and alignments were filtered to include an NGG protospacer-adjacent motif (PAM). Alignments were then mapped to gene coding sequences using the consensus coding sequence (CCDS) database.

## Model fitting

To fit CERES to input data, we solve the following optimization problem:

$$\begin{aligned} \underset{\hat{D}}{\text{minimize}} \quad & \sum_{i=1}^M \sum_{j=1}^N (D_{ij} - \hat{D}_{ij})^2 + \lambda_g \sum_{k=1}^K \sum_{j=1}^N g_{kj}^2 \\ \text{subject to} \quad & 0 \leq q_i \leq 1, i=1, \dots, M \\ & f_j(C) \leq f_j(C'), \forall C \geq C' \in \mathbb{R}_{\geq 0}, j=1, \dots, N \end{aligned}$$

Where  $\hat{D}_{ij}$  is computed according to Equation (1). The constants  $M$ ,  $N$ , and  $K$  in the objective function are, respectively, the total number of sgRNAs, cell lines, and genes in the dataset. The right-hand term in the objective function acts as a regularizer on the cell-line specific deviation from the shared gene-knockout effect, where the hyperparameter  $\lambda_g$  modulates the strength of the regularization. The first constraint on the model parameters ensures that the guide activity scores are between 0 and 1. The second constraint guarantees that the copy-number effect functions are monotonically decreasing in their arguments. As the objective function is not jointly convex in the model parameters, we fit CERES using alternating least squares, first solving for the gene essentiality scores and copy-number effect parameters with the guide activity scores and offsets held constant, then solving for the guide activity scores and offsets as follows:

### Algorithm 1.1

CERES alternating minimization.

---

```

given  $e > 0$ 
initialize
1. gene-knockout and copy-number effect coefficients  $[g, f] := [0, 0]$ 
2. guide activity scores and offsets  $[q, o] := [1, 0]$ 
repeat
1. Solve for gene-knockout and copy-number effects. Compute optimal parameters  $[g^*, f^*]$ 
2. Update.  $[g^*, f^*] := [g, f]$ 
```

- 
3. Solve for guide activity scores and offsets. Compute optimal parameters  $[q^*, o^*]$
  4. Update.  $[q^*, o^*] := [q^*, o^*]$
  5. Evaluate mean squared error (mse).  $mse_t := \|D - \hat{D}\|^2/MN$
  6. Evaluate decrease in error.  $\Delta mse := mse_t - mse_{t-1}$
  7. Stopping criterion. **quit** if  $\Delta mse < \epsilon$
- 

Due to the presence of constraints, we use numerical optimization techniques to solve for the optimal parameters  $[g^*, f^*]$  and  $[q^*, o^*]$  in steps 1 and 3<sup>28</sup>. Note that we use the bracket notation  $[g, f]$  to indicate that the enclosed parameters are inferred simultaneously as variables in a system of constrained linear equations.

### Spline functions

The piecewise linear spline functions  $f_j$  in the CERES model equations allow for flexible modeling of the characteristic saturation of the copy-number effect at high numbers of cuts. They are implemented with B-spline regression methods and are each parameterized by 25 slope coefficients plus a single intercept parameter. These are inferred directly in the regression that determines the gene-knockout effects. Each spline has an initial knot point at CN = 0. The additional knot points are determined by running average linkage clustering on the CN data for each cell line.

### Hyperparameter optimization and test set evaluation

To improve the generalizability of our model and minimize overfitting of the training data, we regularized the cell line specific gene effects. To find the best value of  $\lambda_g$ , we evaluated the mean squared error (MSE) obtained on a randomly selected held-out validation set (one-tenth of all observations) for each of 25 values of  $\lambda_g$  sampled log-uniformly from the interval [0.01, 1]. After the 25 models were evaluated, the value of  $\lambda_g$  yielding the lowest MSE was used to fit the final model on the full set of observations (Supplementary Fig. 11). The optimized value of  $\lambda_g$  was 0.562, 0.681, and 0.681 for the Avana, GeCKOv2, and Wang2017 datasets, respectively.

### Model complexity

Given a collection of CRISPR screening data, let  $N$  be the number of sgRNAs,  $M$  be the number of cell lines, and  $K$  be the number of targeted genes in the dataset. CERES fits  $KM$  cell line specific gene effect parameters and an additional  $K$  parameters for the shared gene effects. The model also fits  $M(S + 1)$  copy-number effect parameters, where  $S$  is the number of CN segments in each piecewise linear spline, and  $2N$  parameters for the guide activity scores and offsets. Ignoring the degrees of freedom lost by regularization and constraints, CERES takes in  $MN$  data points and fits  $MN(1/N + S/N + 2/M + K/N + K/MN)$  parameters.

### Software and implementation

Matrix operations for the optimization procedure were implemented using the open source C ++ linear algebra library Eigen, version 3.3, available at <http://eigen.tuxfamily.org>. These operations were then wrapped into the R statistical software using the ‘RcppEigen’ package,

downloaded from <http://cran.r-project.org>. The optimization routine and final fit for each dataset were run using Google Cloud Platform services.

### Precision-recall analysis

Precision-recall curves were generated using the sets of common core essential and nonessential genes defined in Hart *et al.*<sup>14</sup>. The best threshold for which greater than 95% of hits are essential genes is calculated for an FDR of 5%. The percentage of all essential genes that score as hits at this threshold is calculated as the recall at 5% FDR.

### Comparison with linear regression

For each cell line, average guide scores were regressed against gene-level copy number data using a linear model. The fit residuals are taken as the LM-corrected gene dependency scores. Precision-recall analysis was performed as above.

### Subsampling analysis

We simulated CERES performance generalization to other dataset sizes by downsampling from the Avana dataset. Specifically, for each number  $p$  in the set {1, 2, 4, 8, 16, 32, 64} we ran  $\frac{342}{p}$  trials (up to rounding), such that each cell line appeared once in each run of size  $p$ . For each  $p$  and each cell line, we evaluated the harmonic mean of precision and recall (referred to as the F1-measure) at the point of equiprobability between the essential and nonessential gene classes. We then compared this number to the F1-measure obtained by running CERES on the full Avana dataset. For  $p < 5$  we fixed all guide activity scores to a value of 1.

### Differential dependency

Differential dependency is calculated as the difference between a single cell line's dependency score for a given gene and the mean score for that gene across all lines screened, and then z-score normalized to that cell line's entire set of differential dependencies to reduce the influence of noisy cell lines. For calculating the fraction of differential dependencies that are amplified or unexpressed, only genes with a negative dependency score in at least one cell line are considered.

### Recurrent chromosome arm amplifications

We called recurrent chromosome arm amplifications for a lineage across the entire CCLE CN dataset. A chromosome arm was called as amplified if the weighted median of copy number segments on that arm was greater than 2.8. Recurrently amplified chromosome arms for a lineage were then defined using a one-tailed Fisher's exact test to test for enrichment of amplified arms in that lineage, at an FDR-corrected p-value of 0.05.

### Lineage-specific differential dependencies

For every lineage in our dataset with at least five cell lines, we calculate the difference in means in gene dependency between cell lines of that lineage and the rest of the dataset, and assess significance with a two-tailed student's t-test (df=340), for each gene screened.

Differential dependencies are called with a negative effect size at a significance of FDR-

corrected p-value < 0.05. For each chromosome arm that was recurrently amplified for that lineage, we calculate the fraction of significant differential dependencies on that chromosome arm before and after CERES correction.

## Supplementary Material

Refer to Web version on PubMed Central for supplementary material.

## Acknowledgments

This work was supported by U01 CA176058, U01 CA199253, and P01 CA154303 grants (W.C.Hahn) and by the Slim Initiative for Genomic Medicine, a project funded by the Carlos Slim Foundation and the H.L. Snyder Foundation.

## References

1. Wang T, et al. Identification and characterization of essential genes in the human genome. *Science*. 2015; 350:1096–1101. [PubMed: 26472758]
2. Hart T, et al. High-Resolution CRISPR Screens Reveal Fitness Genes and Genotype-Specific Cancer Liabilities. *Cell*. 2015; 163:1515–1526. [PubMed: 26627737]
3. Aguirre AJ, et al. Genomic Copy Number Dictates a Gene-Independent Cell Response to CRISPR/Cas9 Targeting. *Cancer Discov*. 2016; 6:914–929. [PubMed: 27260156]
4. Munoz DM, et al. CRISPR Screens Provide a Comprehensive Assessment of Cancer Vulnerabilities but Generate False-Positive Hits for Highly Amplified Genomic Regions. *Cancer Discov*. 2016; 6:900–913. [PubMed: 27260157]
5. Cheung HW, et al. Systematic investigation of genetic vulnerabilities across cancer cell lines reveals lineage-specific dependencies in ovarian cancer. *Proc Natl Acad Sci USA*. 2011; 108:12372–12377. [PubMed: 21746896]
6. Marcotte R, et al. Essential gene profiles in breast, pancreatic, and ovarian cancer cells. *Cancer Discov*. 2012; 2:172–189. [PubMed: 22585861]
7. Cowley GS, et al. Parallel genome-scale loss of function screens in 216 cancer cell lines for the identification of context-specific genetic dependencies. *Scientific Data*. 2014; 1:140035. [PubMed: 25984343]
8. Tzelepis K, et al. A CRISPR Dropout Screen Identifies Genetic Vulnerabilities and Therapeutic Targets in Acute Myeloid Leukemia. *Cell Reports*. 2016; 17:1193–1205. [PubMed: 27760321]
9. Wang T, et al. Gene Essentiality Profiling Reveals Gene Networks and Synthetic Lethal Interactions with Oncogenic Ras. *Cell*. 2017; doi: 10.1016/j.cell.2017.01.013
10. Tsherniak A, et al. Defining a Cancer Dependency Map. *Cell*. 2017; 170:564–570.e16. [PubMed: 28753430]
11. Fellmann C, Gowen BG, Lin P-C, Doudna JA, Corn JE. Cornerstones of CRISPR-Cas in drug discovery and therapy. *Nat Rev Drug Discov*. 2016; doi: 10.1038/nrd.2016.238
12. Corsello SM, et al. The Drug Repurposing Hub: a next-generation drug library and information resource. *Nature Medicine*. 2017; 23:405–408.
13. Doench JG, et al. Optimized sgRNA design to maximize activity and minimize off-target effects of CRISPR-Cas9. *Nat Biotechnol*. 2016; 34:184–191. [PubMed: 26780180]
14. Hart T, Brown KR, Sircoulomb F, Rottapel R, Moffat J. Measuring error rates in genomic perturbation screens: gold standards for human functional genomics. *Mol Syst Biol*. 2014; 10:733–733. [PubMed: 24987113]
15. Barretina J, et al. The Cancer Cell Line Encyclopedia enables predictive modelling of anticancer drug sensitivity. *Nature*. 2012; 483:603–607. [PubMed: 22460905]
16. Li W, et al. MAGeCK enables robust identification of essential genes from genome-scale CRISPR/Cas9 knockout screens. *Genome Biol*. 2014; 15:554. [PubMed: 25476604]

17. Hart T, Moffat J. BAGEL: a computational framework for identifying essential genes from pooled library screens. *BMC Bioinformatics*. 2016; 17:164. [PubMed: 27083490]
18. Doench JG, et al. Rational design of highly active sgRNAs for CRISPR-Cas9-mediated gene inactivation. *Nat Biotechnol*. 2014; 32:1262–1267. [PubMed: 25184501]
19. Xu H, et al. Sequence determinants of improved CRISPR sgRNA design. *Genome Res*. 2015; 25:1147–1157. [PubMed: 26063738]
20. Tsherniak A, Vazquez F, Golub TR, Boehm JS, Hahn WC. Defining a Cancer Dependency Map. *Cell*. 2017; :1–31. DOI: 10.1016/j.cell.2017.06.010
21. Xiang X, et al. Grhl2 Determines the Epithelial Phenotype of Breast Cancers and Promotes Tumor Progression. *PLoS ONE*. 2012; 7:e50781. [PubMed: 23284647]
22. Werner S, et al. Dual roles of the transcription factor grainyhead-like 2 (GRHL2) in breast cancer. *J Biol Chem*. 2013; 288:22993–23008. [PubMed: 23814079]
23. Zhang XD. A pair of new statistical parameters for quality control in RNA interference high-throughput screening assays. *Genomics*. 2007; 89:552–561. [PubMed: 17276655]
24. Kanehisa M, Goto S. KEGG: kyoto encyclopedia of genes and genomes. *Nucleic Acids Res*. 2000; 28:27–30. [PubMed: 10592173]
25. Kanehisa M, Sato Y, Kawashima M, Furumichi M, Tanabe M. KEGG as a reference resource for gene and protein annotation. *Nucleic Acids Res*. 2016; 44:D457–62. [PubMed: 26476454]
26. Kanehisa M, Furumichi M, Tanabe M, Sato Y, Morishima K. KEGG: new perspectives on genomes, pathways, diseases and drugs. *Nucleic Acids Res*. 2017; 45:D353–D361. [PubMed: 27899662]
27. Langmead B, Trapnell C, Pop M, Salzberg SL. Ultrafast and memory-efficient alignment of short DNA sequences to the human genome. *Genome Biol*. 2009; 10:R25. [PubMed: 19261174]
28. Boyd, S., Vandenberghe, L. Convex Optimization. Cambridge University Press; 2004. p. 1-730.

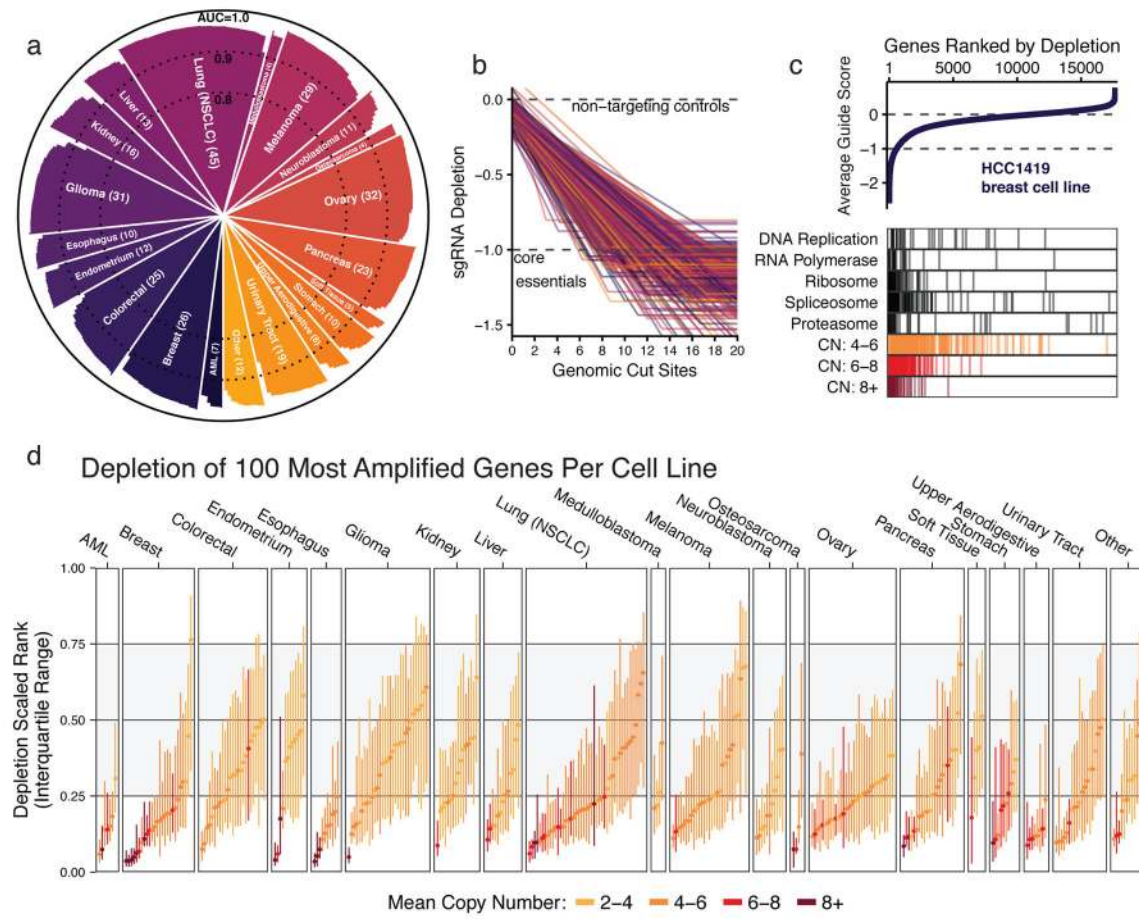


**Figure 1. Genomic copy number confounds the interpretation of CRISPR-Cas9 loss-of-function proliferation screens of cancer cell lines**

(a) Screen quality for each cell line in the panel ( $n=342$ ), as measured by area under the receiver operating characteristic curve (AUC) in discriminating between predefined sets of common core essential and nonessential genes. (b) The depletion of sgRNAs is regressed against the number of perfect-match genomic cut sites using a simple saturating linear fit, which is plotted for each cell line, colored by lineage, and scaled such that the median of sgRNAs targeting cell-essential genes is at  $-1$ , marked by a dashed line. (c) Genes are ranked by the mean depletion of targeting sgRNAs (average guide score) and plotted for an example cell line. Values of  $0$  and  $-1$  represent the median scores of nonessential and cell-essential genes, respectively, indicated by dashed lines. Below, depletion ranks of genes involved in fundamental cell processes and genes at various ranges of CN amplification are shown. (d) The median and interquartile range (IQR) of depletion ranks for the 100 most amplified genes per cell line are plotted. Color indicates mean amplification level of these genes. The gray-shaded area indicates the IQR of all genes screened.

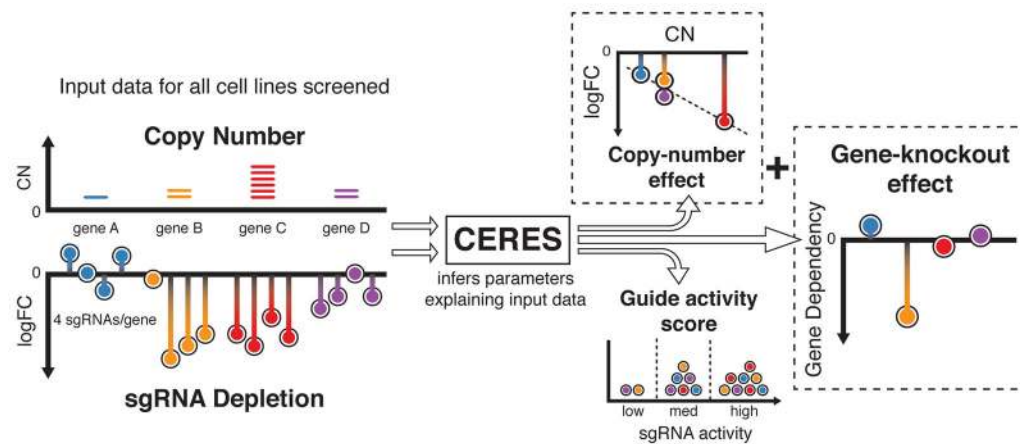


**Figure 2. Schematic of the CERES computational model**

As input, CERES takes sgRNA depletion and CN data for all cell lines screened. During the inference procedure, CERES models the depletion values as a sum of gene-knockout and copy-number effects, multiplied by a guide activity score parameter. CERES then outputs the values of the parameters that produce the highest likelihood of the observed data under the model.

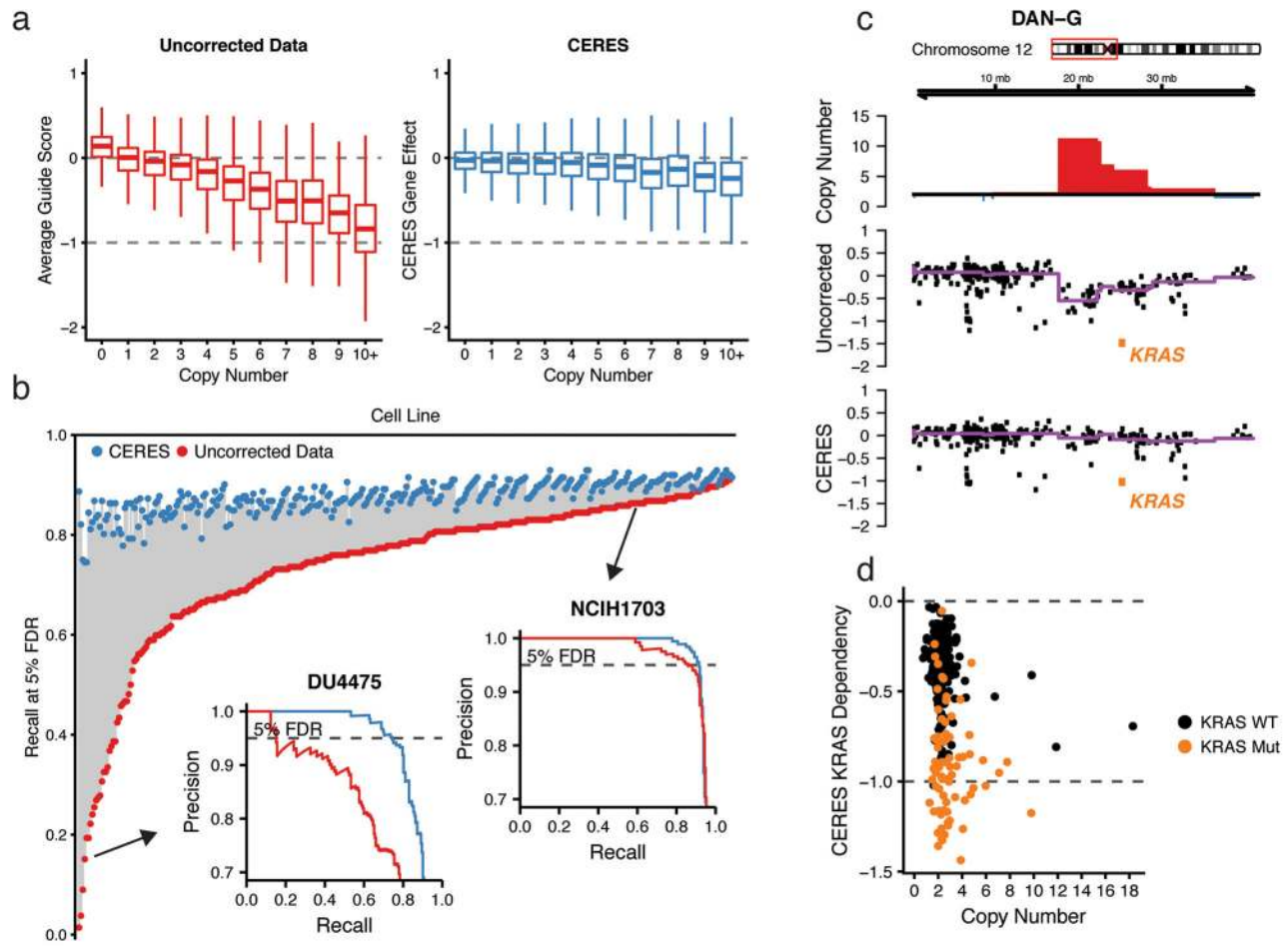


**Figure 3. CERES corrects the copy-number effect and improves the specificity of fCRISPR-Cas9 essentiality screens while preserving true gene dependencies**

(a) Boxplots of gene dependency scores are shown across CN for uncorrected average guide scores and CERES gene dependency scores. Data are scaled as in Fig. 1c. (b) The recall of cell-essential genes at a 5% FDR of nonessential genes is plotted for each cell line before (red) and after (blue) CERES correction. Precision-recall curves are inset for example cell lines with poor recall (bottom left) and good recall (top right) before CERES correction. (c) An example amplified region on chromosome 12p is shown for the DAN-G pancreatic cell line. The top track represents CN with amplifications shown in red. The middle track and bottom tracks show the average guide score and CERES score, respectively, for each gene in this region. The purple line is representing the median value in each CN segment. *KRAS* is highlighted in orange. (d) *KRAS* gene dependency and CN are shown for all cell lines after CERES correction, with mutant *KRAS* lines in orange.

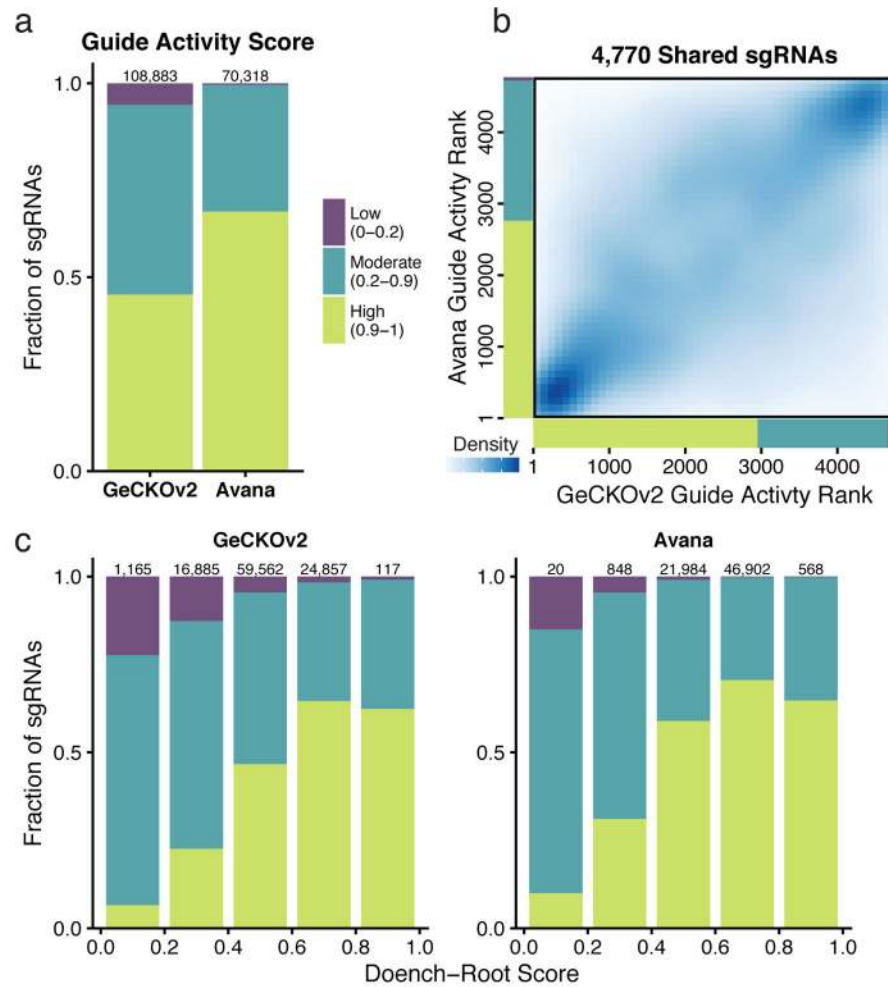


**Figure 4. CERES estimates guide activity scores for each sgRNA**

(a) sgRNAs are binned into groups with high (0.9–1), moderate (0.2–0.9), and low (0–0.2) guide activity scores. The compositions of guide activity scores are shown for the set of screens performed with the GeCKOv2 and the Avana sgRNA libraries. (b) For the set of 4,770 sgRNAs shared between the GeCKOv2 and Avana libraries, sgRNAs are ranked by guide activity scores in each dataset and are plotted against each other, with darker blue representing a greater density of sgRNAs. (c) sgRNAs are binned by predicted on-target activity using the Doench-Root score, and the composition of CERES-estimated guide activity scores is shown for each dataset.

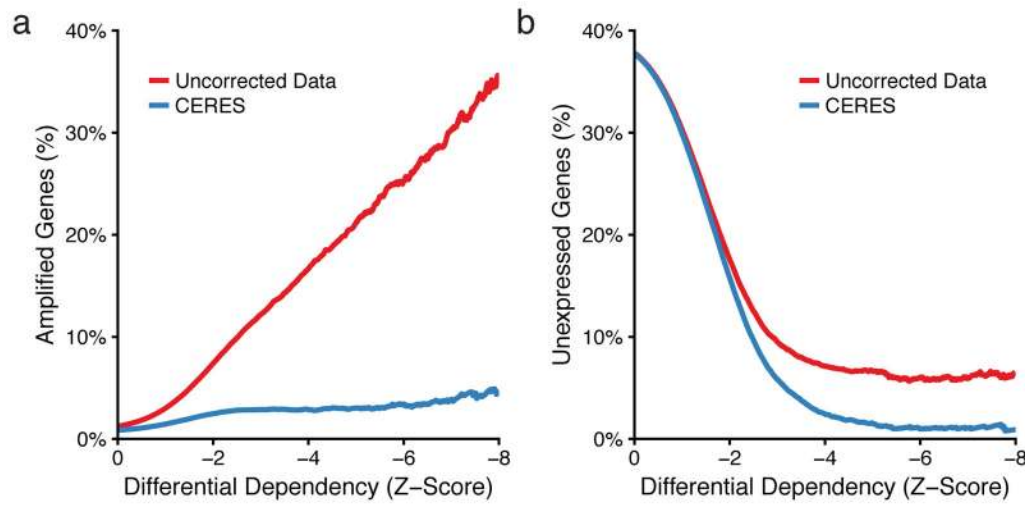


**Figure 5. CERES reduces false positive differential dependencies**

(a) The percentage of genes on amplified regions ( $\text{CN} > 4$ ) below a given differential dependency threshold is plotted for the uncorrected average guide score in red and the CERES gene dependency score in blue. (b) The percentage of unexpressed genes ( $\log_2 \text{RPKM} < -1$ ) below a given differential dependency score is plotted as in (a).

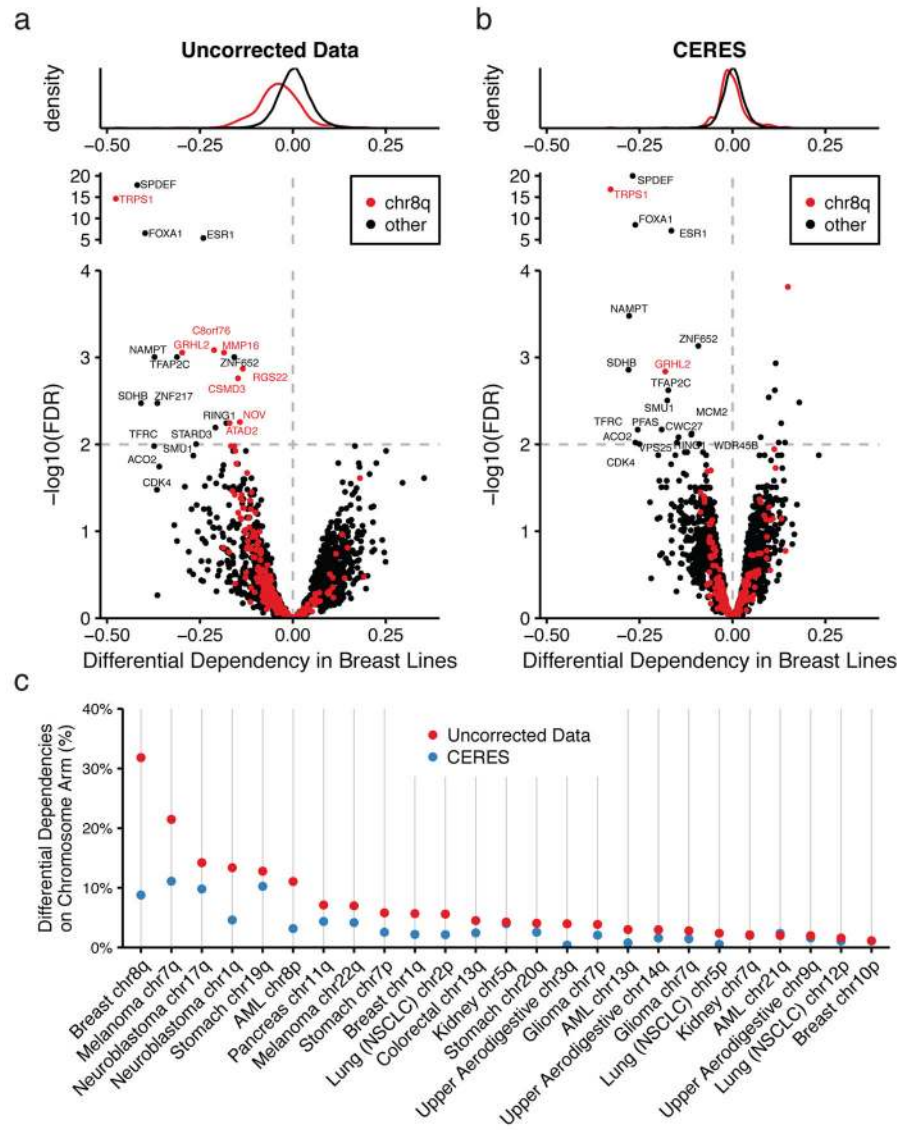


**Figure 6. CERES reduces false positives among lineage-specific differential dependencies due to recurrently amplified chromosome arms**

(a) The distributions of differential dependencies in breast lines are plotted red for genes on chromosome 8q (commonly gained in breast tumors) and black for all other genes. Below, the differential dependency of each gene is plotted against the FDR-corrected p-value, calculated from a student's t-test, with colors as above. The dashed line represents an FDR of 5%. (b) Data are shown for CERES-inferred gene effects as in (a). (c) The percentages of lineage-specific differential dependencies (FDR < 0.05) that are on recurrently amplified chromosome arms are shown, before and after CERES correction.

**Table 1**

Name	Source	Lineage	Histology	Gender	Age	Primary/Metastasis	Achilles culture medium
143B_BONE	CCLE	Osteosarcoma	osteosarcoma	female	13	primary	EMEM; 10% FBS; 0.015 mg/ml 5-bromo-2'-seoxyuridine
42MGBA_CENTRAL_NERVOUS_SYSTEM	CCLE	Glioma	glioma	NA	NA	NA	RPMI 1640 + EMEM (1:1); 80.0%
5637_URINARY_TRACT	CCLE	Urinary Tract	carcinoma	NA	NA	NA	RPMI 1640; 90.0%
59M_OVARY	CCLE	Ovary	carcinoma	NA	NA	NA	"DMEM; 10% FBS + 2 mM Glutamine, sodium pyruvate, ITS"
639V_URINARY_TRACT	CCLE	Urinary Tract	carcinoma	NA	NA	NA	DMEM; 10% FBS
647V_URINARY_TRACT	CCLE	Urinary Tract	carcinoma	NA	NA	NA	"DMEM; 1.5% FBS, 2mMGlutamax-1"
769P_KIDNEY	CCLE	Kidney	carcinoma	female	63	primary	RPMI; 10% FBS
786O_KIDNEY	CCLE	Kidney	carcinoma	male	58	primary	RPMI; 10% FBS
8305C_THYROID	CCLE	Thyroid	carcinoma	NA	NA	NA	RPMI 1640; 85.0%
8MGBA_CENTRAL_NERVOUS_SYSTEM	CCLE	Glioma	glioma	NA	NA	NA	EMEM; 80.0%
A2058_SKIN	CCLE	Melanoma	malignant_melanoma	male	43	metastasis	DMEM; 10% FBS
A2780_OVARY	CCLE	Ovary	carcinoma	female	NA	primary	RPMI; 10% FBS
A549_LUNG	CCLE	Lung (NSCLC)	carcinoma	male	58	primary	DMEM; 10% FBS
ABCl_LUNG	CCLE	Lung (NSCLC)	carcinoma	male	47	primary	EMEM; 10% FBS
AGS_STOMACH	CCLE	Stomach	carcinoma	female	54	primary	F12K; 10% FBS
ASPC1_PANCREAS	CCLE	Pancreas	carcinoma	female	62	metastasis	RPMI; 10% FBS
AU565_BREAST	CCLE	Breast	carcinoma	female	43	metastasis	DMEM; 10% FBS
BC3C_URINARY_TRACT	CCLE	Urinary Tract	carcinoma	NA	NA	NA	M10
BFTC905_URINARY_TRACT	CCLE	Urinary Tract	carcinoma	NA	NA	NA	DMEM; 90.0%
BFTC99_KIDNEY	CCLE	Kidney	carcinoma	male	64	primary	DMEM; 10% FBS
BHY_UPPER_AERODIGESTIVE_TRACT	CCL	Upper Aerodigestive	carcinoma	male	NA	NA	DMEM; 10% FBS
BICR22_UPPER_AERODIGESTIVE_TRACT	CCL	Upper Aerodigestive	carcinoma	male	NA	primary	DMEM; 10% FBS; 2mM Glutamine; 0.4ug/ml hydrocortisone
BICR6_UPPER_AERODIGESTIVE_TRACT	CCL	Upper Aerodigestive	carcinoma	male	NA	NA	DMEM; 10% FBS
BT549_BREAST	CCL	Breast	carcinoma	female	72	primary	RPMI; 10% FBS; 10 ug/ml insulin
C2BBE1_LARGE_INTESTINE	CCL	Colorectal	carcinoma	male	72	primary	DMEM; 10% FBS; 0.01mg/ml transferrin; 2 mM glutamine
C32_SKIN	CCL	Melanoma	malignant_melanoma	male	53	primary	EMEM; 10% FBS; 0.1mM NEAA
CAKII_KIDNEY	CCL	Kidney	carcinoma	male	49	metastasis	McCoy's 5A; 10% FBS
CAKII_KIDNEY	CCL	Kidney	carcinoma	male	69	primary	McCoy's 5A; 10% FBS
CAL27_UPPER_AERODIGESTIVE_TRACT	CCL	Upper Aerodigestive	carcinoma	male	56	primary	DMEM; 10% FBS
CAL29_URINARY_TRACT	CCL	Urinary Tract	carcinoma	NA	NA	NA	DMEM; 10% FBS

Name	Source	Lineage	Histology	Gender	Age	Primary/Metastasis	Achilles culture medium
CAL51_BREAST	CCLE	Breast	carcinoma	female	45	metastasis	DMEM; 20% FBS
CAL78_BONE	CCLE	Chondrosarcoma	chondrosarcoma	NA	NA	NA	"RPMI-1640, 20% FBS"
CALU6_LUNG	CCLE	Lung (NSCLC)	carcinoma	female	61	primary	EMEM; 10% FBS
CAMA1_BREAST	CCLE	Breast	carcinoma	female	51	metastasis	EMEM; 10% FBS
CAOV3_OVARY	CCLE	Ovary	carcinoma	female	54	primary	DMEM; 10% FBS
CAS1_CENTRAL_NERVOUS_SYSTEM	CCLE	Glioma	glioma	male	63	primary	DMEM; 10% FBS
CCFSTTGL_CENTRAL_NERVOUS_SYSTEM	CCLE	Glioma	glioma	NA	NA	NA	RPMI; 10% FBS
CCK81_LARGE_INTESTINE	CCLE	Colorectal	carcinoma	NA	NA	NA	"EMEM, 10% FBS"
CFPAC1_PANCREAS	CCLE	Pancreas	carcinoma	male	26	primary	DMEM; 10% FBS
CHAGOK1_LUNG	CCLE	Lung (NSCLC)	carcinoma	male	45	primary	RPMI; 10% FBS; 2mM glutamine
CHP212_AUTONOMIC_GANGLIA	CCLE	Neuroblastoma	neuroblastoma	NA	NA	NA	EMEM: F12 (1:1); 10% FBS
CIM_SKIN	CCLE	Melanoma	malignant_melanoma	NA	NA	metastasis	Hans F-12; 10% FBS
CL40_LARGE_INTESTINE	CCLE	Colorectal	carcinoma	NA	NA	NA	"DMEM/F-12 (1:1), 20% FBS"
COLO678_LARGE_INTESTINE	CCLE	Colorectal	carcinoma	male	NA	NA	RPMI; 10% FBS
COLO679_SKIN	CCLE	Melanoma	malignant_melanoma	female	47	metastasis	RPMI; 10% FBS
COL0792_SKIN	CCLE	Melanoma	malignant_melanoma	male	62	metastasis	RPMI; 10% FBS
COLO800_SKIN	CCLE	Melanoma	malignant_melanoma	male	14	primary	RPMI-1640; 10%FBS
CORL279_LUNG	CCLE	Lung (SCL)	carcinoma	male	63	metastasis	RPMI; 10% FBS; 2mM glutamine
CORL47_LUNG	CCLE	Lung (SCL)	carcinoma	NA	NA	NA	RPMI; 10% FBS
COV318_OVARY	CCLE	Ovary	carcinoma	female	NA	primary	EMEM; 10% FBS
COV362_OVARY	CCLE	Ovary	carcinoma	female	NA	primary	DMEM; 10% FBS; 2mM L-glutamine
COV434_OVARY	CCLE	Ovary	sex_cord-stromal_tumour	female	NA	primary	DMEM; 10% FBS; 2mM L-glutamine
COV504_OVARY	CCLE	Ovary	carcinoma	female	NA	primary	DMEM; 10% FBS; 2mM L-glutamine
D283MED_CENTRAL_NERVOUS_SYSTEM	CCLE	Medulloblastoma	primitive_neuroectodermal_tumour-medulloblastoma	male	NA	NA	"DMEM; 10% FBS; 2mM L-glutamine, 2mM sodium pyruvate"
D341MED_CENTRAL_NERVOUS_SYSTEM	CCLE	Medulloblastoma	primitive_neuroectodermal_tumour-medulloblastoma	male	NA	NA	DMEM: F12 (1:1; 15% FBS
DANG_PANCREAS	CCLE	Pancreas	carcinoma	NA	NA	NA	RPMI-1640; 90.0%
DAOY_CENTRAL_NERVOUS_SYSTEM	CCLE	Medulloblastoma	primitive_neuroectodermal_tumour-medulloblastoma	NA	NA	NA	EMEM: 90.0% 10%FBS
DETROIT562_UPPER_AERODIGESTIVE_TRACT	CCLE	Upper Aerodigestive	carcinoma	female	NA	NA	EMEM; 10% FBS
DKMG_CENTRAL_NERVOUS_SYSTEM	CCLE	Glioma	glioma	female	67	primary	RPMI; 10% FBS; 2mM glutamine
DLD1_LARGE_INTESTINE	CCLE	Colorectal	carcinoma	male	NA	primary	RPMI; 10% FBS

Name	Source	Lineage	Histology	Gender	Age	Primary/Metastasis	Achilles culture medium
DU4475_BREAST	CCLE	Breast	carcinoma	female	70	metastasis	RPMI; 10% FBS
EFM19_BREAST	CCLE	Breast	carcinoma	female	50	metastasis	RPMI; 10% FBS
EF021_OVARY	CCLE	Ovary	carcinoma	female	56	metastasis	RPMI; 20% FBS; 0.1mM NEAA; 1mM Sodium Pyruvate
EF027_OVARY	CCLE	Ovary	carcinoma	female	36	metastasis	RPMI; 20% FBS; 0.1mM NEAA; 1mM Sodium Pyruvate
EKVK_LUNG	CCLE	Lung (NSCLC)	carcinoma	NA	NA	primary	RPMI; 10% FBS
EPLC27H_LUNG	CCLE	Lung (NSCLC)	carcinoma	male	57	primary	RPMI; 20% FBS
ES2_OVARY	CCLE	Ovary	carcinoma	female	47	primary	RPMI; 10% FBS
ESS1_ENDOMETRIUM	CCLE	Endometrium	carcinoma	female	76	primary	RPMI; 20% FBS
F5_CENTRAL_NERVOUS_SYSTEM	“Dunn Lab, Harvard”	Meningioma	meningioma	male	NA	NA	RPMI; 10% FBS
FADU_UPPER_AERODIGESTIVE_TRACT	CCLE	Upper Aerodigestive	carcinoma	male	NA	NA	EMEM; 10% FBS
FU97_STOMACH	CCLE	Stomach	carcinoma	female	NA	NA	DMEM; 10% FBS; Human Insulin: 0.01 mg/mL
G292CLONEA141B1_BONE	CCLE	Osteosarcoma	osteosarcoma	NA	NA	NA	McCoy's 5A; 10% FBS
G401_SOFT_TISSUE	CCLE	Soft Tissue	rhabdoid_tumour	male	0.25	primary	McCoy's 5A; 10% FBS
GAMG_CENTRAL_NERVOUS_SYSTEM	CCLE	Glioma	glioma	NA	NA	NA	DMEM; 10%FBS, 2mM Glutamax-1 <sup>+</sup>
GB1_CENTRAL_NERVOUS_SYSTEM	CCLE	Glioma	glioma	male	35	primary	EMEM; 10% FBS
GCIY_STOMACH	CCLE	Stomach	carcinoma	female	NA	primary	MEM; 15% FBS
GH1_CENTRAL_NERVOUS_SYSTEM	CCLE	Glioma	glioma	NA	NA	NA	DMEM; 90.0%
GSS_STOMACH	CCLE	Stomach	carcinoma	NA	NA	NA	RPMI; 10% FBS
H4_CENTRAL_NERVOUS_SYSTEM	CCLE	Glioma	glioma	NA	NA	NA	DMEM: 90.0%
HARA_LUNG	CCLE	Lung (NSCLC)	carcinoma	male	57	primary	RPMI; 10% FBS
HCC1143_BREAST	CCLE	Breast	carcinoma	female	52	primary	RPMI; 10% FBS
HCC1359_LUNG	CCLE	Lung (NSCLC)	carcinoma	female	55	primary	RPMI; 10% FBS
HCC1395_BREAST	CCLE	Breast	carcinoma	female	43	primary	RPMI; 10% FBS
HCC1419_BREAST	CCLE	Breast	carcinoma	NA	NA	NA	RPMI-1640; 90.0%
HCC1428_BREAST	CCLE	Breast	carcinoma	female	49	metastasis	RPMI; 10% FBS
HCC15_LUNG	CCLE	Lung (NSCLC)	carcinoma	male	47	primary	RPMI; 10% FBS
HCC1806_BREAST	CCLE	Breast	carcinoma	female	60	primary	RPMI; 10% FBS
HCC1937_BREAST	CCLE	Breast	carcinoma	female	24	primary	RPMI; 10% FBS
HCC1954_BREAST	CCLE	Breast	carcinoma	female	61	primary	RPMI; 10% FBS
HCC202_BREAST	CCLE	Breast	carcinoma	female	82	primary	RPMI; 10% FBS
HCC36_LARGE_INTESTINE	CCLE	Colorectal	carcinoma	NA	NA	NA	EMEM; 10% FBS

Name	Source	Lineage	Histology	Gender	Age	Primary/Metastasis	Achilles culture medium
HCC827_LUNG	CCLE	Lung (NSCLC)	carcinoma	female	39	primary	RPMI; 10% FBS
HCC95_LUNG	CCLE	Lung (NSCLC)	carcinoma	male	65	primary	RPMI; 10% FBS
HEC1A-ENDOMETRIUM	CCLE	Endometrium	carcinoma	female	71	primary	McCoy's 5A; 10% FBS
HEC1B-ENDOMETRIUM	CCLE	Endometrium	carcinoma	NA	NA	NA	EMEM; 10% FBS
HEC251-ENDOMETRIUM	CCLE	Endometrium	carcinoma	female	NA	primary	EMEM; 0.15% FBS
HEC50B-ENDOMETRIUM	CCLE	Endometrium	carcinoma	female	NA	primary	EMEM; 15% FBS
HEC59-ENDOMETRIUM	CCLE	Endometrium	carcinoma	female	NA	primary	EMEM; 0.15% FBS
HEC6-ENDOMETRIUM	CCLE	Endometrium	carcinoma	NA	NA	NA	EMEM; 15% FBS
HEYA8_OVARY	CCLE	Ovary	carcinoma	female	NA	primary	RPMI; 10% FBS
HGC27_STOMACH	CCLE	Stomach	carcinoma	NA	NA	NA	Minimum Essential Media (MEM); 10% FBS; NEAA (Non-essential Amino Acids); 5.0 mM; L-glutamine; 2.0 mM EMEM; 10% FBS
HLF_LIVER	CCLE	Liver	carcinoma	male	69	primary	EMEM; 10% FBS
HMC18_BREAST	CCLE	Breast	carcinoma	NA	NA	NA	RPMI-1640; 10%FBS
HOP62_LUNG	CCLE	Lung (NSCLC)	carcinoma	NA	NA	primary	RPMI; 10% FBS
HS294T_SKIN	CCLE	Melanoma	malignant_melanoma	male	56	metastasis	DMEM; 10% FBS
HS578T_BREAST	CCLE	Breast	carcinoma	female	74	primary	DMEM; 10% FBS
HS683_CENTRAL_NERVOUS_SYSTEM	CCLE	Glioma	glioma	male	76	primary	DMEM; 10% FBS
HS695T_SKIN	CCLE	Melanoma	malignant_melanoma	male	NA	NA	EMEM; 10% FBS
HS729_SOFT_TISSUE	CCLE	Soft Tissue	rhabdomyosarcoma	NA	NA	NA	DMEM; 5% FBS
HS766T_PANCREAS	CCLE	Pancreas	carcinoma	male	46	primary	DMEM; 10% FBS
HS944T_SKIN	CCLE	Melanoma	malignant_melanoma	male	51	metastasis	DMEM; 10% FBS
HSC3_UPPER_AERODIGESTIVE_TRACT	CCLE	Upper Aerodigestive	carcinoma	male	64	primary	EMEM; 10% FBS
HT1080_SOFT_TISSUE	CCLE	Soft Tissue	fibrosarcoma	male	35	metastasis	EMEM; 10% FBS
HT115_LARGE_INTESTINE	CCLE	Colorectal	carcinoma	NA	NA	NA	DMEM; 15% FBS; 2mM Glutamax-1
HT1197_URINARY_TRACT	CCLE	Urinary Tract	carcinoma	male	44	primary	EMEM; 10% FBS
HT1376_URINARY_TRACT	CCLE	Urinary Tract	carcinoma	NA	NA	NA	EMEM; 10% FBS
HT144_SKIN	CCLE	Melanoma	malignant_melanoma	male	NA	NA	McCoy's 5A; 10% FBS
HT55_LARGE_INTESTINE	CCLE	Colorectal	carcinoma	NA	NA	primary	EMEM; 20% FBS; 2mM L-glutamine; 0.1mM NEAA
HUH1_LIVER	CCLE	Liver	carcinoma	male	35	primary	DMEM; 10% FBS
HUH6_LIVER	CCLE	Liver	other	NA	NA	NA	DMEM; 10% FBS
HUH7_LIVER	CCLE	Liver	carcinoma	male	57	primary	DMEM; 10% FBS
HUPT3_PANCREAS	CCLE	Pancreas	carcinoma	male	66	primary	MEM; 10% FBS

Name	Source	Lineage	Histology	Gender	Age	Primary/Metastasis	Achilles culture medium
IGR1_SKIN	CCLE	Melanoma	malignant_melanoma	male	42	metastasis	DMEM; 10% FBS
IGR39_SKIN	CCLE	Melanoma	malignant_melanoma	male	26	primary	DMEM; 15% FBS
IMR32_AUTONOMIC_GANGLIA	CCLE	Neuroblastoma	neuroblastoma	male	NA	NA	EMEM; 10% FBS
IPC298_SKIN	CCLE	Melanoma	malignant_melanoma	female	64	primary	RPMI; 10% FBS
JHH1_LIVER	CCLE	Liver	carcinoma	male	50	primary	William's E Medium; 10% FBS
JHH4_LIVER	CCLE	Liver	carcinoma	NA	NA	NA	EMEM; 10% FBS
JHH5_LIVER	CCLE	Liver	carcinoma	male	50	primary	William's E Medium; 90.0%
JHH7_LIVER	CCLE	Liver	carcinoma	NA	NA	NA	William's E medium with 10% FCS
JHOC5_OVARY	CCLE	Ovary	carcinoma	female	NA	primary	DMEM:FI2 (1:1); 10% FBS; 0.1mM NEAA
JHOM1_OVARY	CCLE	Ovary	carcinoma	female	NA	primary	DMEM:FI2 (1:1); 10% FBS; 0.1mM NEAA
JHOS2_OVARY	CCLE	Ovary	carcinoma	female	45	primary	DMEM:FI2 (1:1); 10 % FBS;
JHOS4_OVARY	CCLE	Ovary	carcinoma	female	44	primary	DMEM:FI2 (1:1); 10% FBS
JIMT1_BREAST	CCLE	Breast	carcinoma	NA	NA	NA	RPMI; 10% FBS
JMSU1_URINARY_TRACT	CCLE	Urinary Tract	carcinoma	NA	NA	NA	RPMI; 10% FBS; 2mM Glutamax-1
K029AX_SKIN	CCLE	Melanoma	malignant_melanoma	NA	NA	primary	RPMI; 10% FBS
KALSL_CENTRAL_NERVOUS_SYSTEM	CCLE	Glioma	glioma	female	NA	primary	RPMI; 5% FBS
KARPAS299_HAEMATOPOIETIC_ANDLYMPHOID	CCLE	Neuroblastoma	ALCLymphoid_neoplasm	male	NA	NA	"RPMI, 20% FBS, 2 mM L-glutamine"
KELLY_AUTONOMIC_GANGLIA	CCLE	Neuroblastoma	ALCLymphoid_neoplasm	NA	NA	NA	RPMI; 10% FBS
KIK_HAEMATOPOIETIC_ANDLYMPHOID	CCLE	Endometrium	ALCLymphoid_neoplasm	male	NA	NA	RPMI; 20% FBS
KLE_ENDOMETRIUM	CCLE	Colorectal	carcinoma	NA	NA	primary	"DMEM/F-12 (1:1), 10%FBS"
KM12_LARGE_INTESTINE	CCLE	Urinary Tract	carcinoma	NA	NA	NA	RPMI; 10% FBS
KMBC2_URINARY_TRACT	CCLE	Kidney	carcinoma	male	NA	primary	DMEM; 10% FBS
KMRC1_KIDNEY	CCLE	Kidney	carcinoma	NA	NA	primary	DMEM; 10% FBS
KMRC20_KIDNEY	CCLE	Glioma	glioma	NA	NA	NA	EMEM; 5% FBS
KNS42_CENTRAL_NERVOUS_SYSTEM	CCLE	Glioma	glioma	male	55	primary	DMEM; 0.05% FBS
KNS60_CENTRAL_NERVOUS_SYSTEM	CCLE	Lung (NSCLC)	carcinoma	male	49	primary	EMEM; 20% FBS
KNS62_LUNG	CCLE	Glioma	glioma	male	65	primary	DMEM; 5% FBS
KNS81_CENTRAL_NERVOUS_SYSTEM	CCLE	Pancreas	carcinoma	female	65	primary	RPMI; 10% FBS
KP2_PANCREAS	CCLE	Pancreas	carcinoma	NA	NA	NA	RPMI; 10% FBS
KP3_PANCREAS	CCLE	Pancreas	carcinoma	male	50	metastasis	DMEM:F12 (1:1); 10% FBS
KP4_PANCREAS	CCLE	Pancreas	carcinoma				

Name	Source	Lineage	Histology	Gender	Age	Primary/Metastasis	Achilles culture medium
KPL1_BREAST	CCLE	Breast	carcinoma	female	50	metastasis	DMEM; 10% FBS
KPNYN_AUTONOMIC_GANGLIA	CCLE	Neuroblastoma	neuroblastoma	NA	NA	NA	RPMI; 10% FBS
KSL_CENTRAL_NERVOUS_SYSTEM	CCLE	Glioma	glioma	NA	NA	NA	MEM; 10% FBS; 2mMGlutamax-1
KU1919_URINARY_TRACT	CCLE	Urinary Tract	carcinoma	NA	NA	NA	RPMI; 10%heat-inactive FBS
KURAMOCHI_OVARY	CCLE	Ovary	carcinoma	female	NA	primary	RPMI; 10% FBS
KYSE180_OESOPHAGUS	CCLE	Esophagus	carcinoma	male	NA	NA	RPMI; 10% FBS
KYSE270_OESOPHAGUS	CCLE	Esophagus	carcinoma	NA	NA	NA	RPMI:1640:Fl12 (1:1); 90.0%
KYSE30_OESOPHAGUS	CCLE	Esophagus	carcinoma	male	64	primary	RPMI:Fl12 (1:1); 20% FBS
KYSE410_OESOPHAGUS	CCLE	Esophagus	carcinoma	NA	NA	NA	RPMI:1640; 90.0%
KYSE450_OESOPHAGUS	CCLE	Esophagus	carcinoma	male	59	primary	RPMI:HansF-12(1:1) (RPMI-1640 (Hyclone Cat# SH30026.01); 10% FBS SH30027.02);Hans F-12 (Hyclone Cat.# SH30026.01); 10% FBS
KYSE70_OESOPHAGUS	CCLE	Esophagus	carcinoma	male	77	primary	RPMI; 10% FBS
LCLC103H_LUNG	CCLE	Lung (NSCLC)	carcinoma	male	61	metastasis	RPMI; 10% FBS
L17_LIVER	CCLE	Liver	carcinoma	NA	NA	NA	RPMI; 10% FBS
LK2_LUNG	CCLE	Lung (NSCLC)	carcinoma	male	NA	primary	DMEM; 10% FBS
LNI8_CENTRAL_NERVOUS_SYSTEM	CCLE	Glioma	glioma	male	65	primary	DMEM; 5% FBS
LN235_CENTRAL_NERVOUS_SYSTEM	“Lynda Chin, MD Anderson”	Glioma	glioma	male	NA	NA	DMEM; 10% FBS
LN382_CENTRAL_NERVOUS_SYSTEM	“Lynda Chin, MD Anderson”	Glioma	glioma	male	NA	NA	DMEM; 10% FBS
LN443_CENTRAL_NERVOUS_SYSTEM	“Mikael Rinne, DFCI” “Lynda Chin, MD Anderson”	Glioma	glioma	male	NA	NA	DMEM; 10% FBS
LNZ308_CENTRAL_NERVOUS_SYSTEM	“Lynda Chin, MD Anderson”	Glioma	glioma	female	NA	NA	DMEM; 10% FBS
LOVO_LARGE_INTESTINE	CCLE	Colorectal	carcinoma	male	56	metastasis	F12K; 10% FBS
LS1034_LARGE_INTESTINE	CCLE	Colorectal	carcinoma	male	NA	NA	RPMI; 10% FBS
LS180_LARGE_INTESTINE	CCLE	Colorectal	carcinoma	female	NA	NA	EMEM; 10% FBS
LS513_LARGE_INTESTINE	CCLE	Colorectal	carcinoma	male	63	primary	RPMI; 10% FBS
LUDLUI_LUNG	CCLE	Lung (NSCLC)	carcinoma	male	72	primary	RPMI; 10% FBS
LXF289_LUNG	CCLE	Lung (NSCLC)	carcinoma	male	63	primary	Hans F-12; 10% FBS
M059K_CENTRAL_NERVOUS_SYSTEM	CCLE	Glioma	glioma	male	33	primary	DMEM/F12 (1:1); 10 % FBS
MALME3M_SKIN	CCLE	Melanoma	malignant_melanoma	male	43	metastasis	RPMI; 10% FBS
MCAS_OVARY	CCLE	Ovary	carcinoma	NA	NA	NA	EMEM:1.5%FBS
MDAMB157_BREAST	CCLE	Breast	carcinoma	female	44	metastasis	RPMI; 10% FBS

Name	Source	Lineage	Histology	Gender	Age	Primary/Metastasis	Achilles culture medium
MDAMB231_BREAST	CCLE	Breast	carcinoma	female	51	metastasis	RPMI; 10% FBS
MDAMB415_BREAST	CCLE	Breast	carcinoma	female	38	metastasis	L-15; 1.5% FBS; 2mM glutamine; 10mcg/ml Insulin; 10mcg/ml Glutathione
MDAMB435S_SKIN	CCLE	Melanoma	malignant_melanoma	female	NA	NA	RPMI; 10% FBS
MDAMB436_BREAST	CCLE	Breast	carcinoma	female	43	metastasis	RPMI; 10% FBS; 16ug/ml glutathione
MDAMB453_BREAST	CCLE	Breast	carcinoma	female	48	metastasis	RPMI; 10% FBS
MDAMB468_BREAST	CCLE	Breast	carcinoma	female	51	metastasis	DMEM; 10% FBS
MDST8_LARGE_INTESTINE	CCLE	Colorectal	carcinoma	NA	NA	NA	DMEM; 10% FBS; 2mM Glutamine
MELHO_SKIN	CCLE	Melanoma	malignant_melanoma	female	NA	primary	RPMI; 10% FBS
MELUSO_SKIN	CCLE	Melanoma	malignant_melanoma	female	NA	NA	RPMI; 10% FBS
MFE319_ENDOMETRIUM	CCLE	Endometrium	carcinoma	NA	NA	NA	40% RPMI 1640 + 40% MEM (with Earle's salts) + 20% h.i. FBS
MHHNB11_AUTONOMIC_GANGLIA	CCLE	Neuroblastoma	neuroblastoma	male	NA	NA	RPMI; 10% FBS
MIAAPACA2_PANCREAS	CCLE	Pancreas	carcinoma	male	65	primary	DMEM; 10% FBS
MKN45_STOMACH	CCLE	Stomach	carcinoma	female	62	metastasis	RPMI; 10% FBS
MOLM13_HAEMATOPOETIC_AND_LYMPHOID_TISSUE	CCLE	AML	haematopoietic_neoplasm	male	20	primary	RPMI; 20% FBS
MORCPR_LUNG	CCLE	Lung (NSCLC)	carcinoma	NA	NA	primary	RPMI; 10% FBS
MV411_HAEMATOPOETIC_AND_LYMPHOID_TISSUE	CCLE	AML	haematopoietic_neoplasm	male	10	primary	IMDM; 10% FBS
NBL_AUTONOMIC_GANGLIA	CCLE	Neuroblastoma	neuroblastoma	male	NA	NA	RPMI; 10% FBS
NB4_HAEMATOPOETIC_AND_LYMPHOID_TISSUE	CCLE	AML	haematopoietic_neoplasm	female	23	primary	RPMI; 10% FBS
NCHI1299_LUNG	CCLE	Lung (NSCLC)	carcinoma	male	43	metastasis	RPMI; 10% FBS
NCHI1437_LUNG	CCLE	Lung (NSCLC)	carcinoma	male	6	metastasis	RPMI; 10% FBS
NCHI1581_LUNG	CCLE	Lung (NSCLC)	carcinoma	male	44	primary	DMEM:FL12 (1:1); 10% FBS
NCHI1650_LUNG	CCLE	Lung (NSCLC)	carcinoma	male	27	metastasis	RPMI; 10% FBS
NCHI1693_LUNG	CCLE	Lung (NSCLC)	carcinoma	female	55	metastasis	RPMI; 10% FBS
NCHI1703_LUNG	CCLE	Lung (NSCLC)	carcinoma	male	54	primary	RPMI; 10% FBS
NCHI1792_LUNG	CCLE	Lung (NSCLC)	carcinoma	male	50	metastasis	RPMI; 10% FBS
NCHI1944_LUNG	CCLE	Lung (NSCLC)	carcinoma	female	62	metastasis	RPMI; 10% FBS
NCH2023_LUNG	CCLE	Lung (NSCLC)	carcinoma	male	26	metastasis	"DMEM:HAM's FL12 (1:1); 5% FBS; .005 mg/ml insulin, .01 mg/ml transferrin, 30nM sodium selenite, 10 nM hydrocortisone, 10 nM beta estradiol, 10 mM HEPES, 2 mM L-glutamine"
NCH2030_LUNG	CCLE	Lung (NSCLC)	carcinoma	male	NA	metastasis	RPMI; 10% FBS
NCH2087_LUNG	CCLE	Lung (NSCLC)	carcinoma	male	69	metastasis	RPMI; 5% FBS

Name	Source	Lineage	Histology	Gender	Age	Primary/Metastasis	Achilles culture medium
NCH2110_LUNG	CCLE	Lung (NSCLC)	carcinoma	NA	NA	metastasis	RPMI; 10% FBS
NCH2122_LUNG	CCLE	Lung (NSCLC)	carcinoma	female	46	metastasis	RPMI; 10% FBS
NCH2126_LUNG	CCLE	Lung (NSCLC)	carcinoma	male	65	metastasis	"DMEM:HAM's F12 (1:1); 5% FBS; .005 mg/ml insulin, 10 nM mg/ml transferrin, 30nM sodium selenite, 10 nM hydrocortisone, 10 nM beta estradiol, 10 mM HEPES, 2 mM L-glutamine"
NCH2170_LUNG	CCLE	Lung (NSCLC)	carcinoma	male	NA	primary	RPMI; 10% FBS
NCH2172_LUNG	CCLE	Lung (NSCLC)	carcinoma	female	NA	primary	RPMI; 10% FBS
NCH229_LUNG	CCLE	Lung (NSCLC)	carcinoma	male	NA	metastasis	RPMI; 10% FBS
NCH23_LUNG	CCLE	Lung (NSCLC)	carcinoma	male	51	primary	RPMI; 10% FBS
NCH322_LUNG	CCLE	Lung (NSCLC)	carcinoma	male	52	primary	RPMI; 10% FBS; 2mM glutamine
NCH441_LUNG	CCLE	Lung (NSCLC)	carcinoma	male	NA	metastasis	RPMI; 10% FBS
NCH460_LUNG	CCLE	Lung (NSCLC)	carcinoma	male	NA	metastasis	RPMI; 10% FBS
NCH520_LUNG	CCLE	Lung (NSCLC)	carcinoma	male	NA	primary	RPMI; 10% FBS
NCH716_LARGE_INTESTINE	CCLE	Colorectal	carcinoma	male	33	metastasis	RPMI; 10% FBS
NCH747_LARGE_INTESTINE	CCLE	Colorectal	carcinoma	male	69	metastasis	RPMI; 10% FBS
NCH838_LUNG	CCLE	Lung (NSCLC)	carcinoma	male	59	metastasis	RPMI; 10% FBS
NCIN87_STOMACH	CCLE	Stomach	carcinoma	male	NA	metastasis	RPMI; 10% FBS
NOMO1_HAEMATOPOIETIC_AND_LYMPHOID_TISSUE	CCLE	AML	haematopoietic_neoplasm	female	31	primary	RPMI; 10% FBS
NUGC3_STOMACH	CCLE	Stomach	carcinoma	male	72	primary	RPMI; 10% FBS
OAW28_OVARY	CCLE	Ovary	carcinoma	NA	NA	NA	DMEM; 10% FBS
OE21_OESOPHAGUS	CCLE	Esophagus	carcinoma	NA	NA	NA	RPMI-1640; 90.0%
OE33_OESOPHAGUS	CCLE	Esophagus	other	female	73	primary	RPMI; 10% FBS
ONS76_CENTRAL_NERVOUS_SYSTEM	CCLE	Medulloblastoma	primitive_neuroectodermal_tumour-medulloblastoma	NA	NA	NA	RPMI; 10% FBS
OSRC2_KIDNEY	CCLE	Kidney	carcinoma	NA	NA	primary	RPMI; 10% FBS
OUMS23_LARGE_INTESTINE	CCLE	Colorectal	carcinoma	NA	NA	NA	DMEM; 10% FBS
OV7_OVARY	CCLE	Ovary	carcinoma	female	78	primary	DMEM:F12 (1:1); 5% FBS; 2mM L-glutamine; 0.5ug/ml hydrocortisone; 10ug/ml insulin
OV90_OVARY	CCLE	Ovary	carcinoma	female	64	metastasis	DMEM; 10% FBS (Tony) 1:1 mixture of MCDB 105 medium with 1.5 g/L sodium bicarbonate added and Medium 199; 10% FBS]
OVCAR8_OVARY	CCLE	Ovary	carcinoma	female	64	primary	RPMI; 10% FBS
OVISE_OVARY	CCLE	Ovary	carcinoma	female	40	primary	RPMI; 10% FBS
OVK18_OVARY	CCLE	Ovary	carcinoma	NA	NA	NA	MEM10

Name	Source	Lineage	Histology	Gender	Age	Primary/Metastasis	Achilles culture medium
OVMANA_OVARY	CCLE	Ovary	carcinoma	female	51	primary	RPMI; 10% FBS
OVTOKO_OVARY	CCLE	Ovary	carcinoma	female	78	metastasis	RPMI; 10% FBS
P31FUI_HAEMATOPOIETIC_AND_LYMPHOID_TISSUE	CCLE	AML	haematopoietic_neoplasm	male	NA	NA	RPMI; 10% FBS
PANC0203_PANCREAS	CCLE	Pancreas	carcinoma	female	NA	NA	RPMI; 10% FBS; 1mM sodium pyruvate
PANC0403_PANCREAS	CCLE	Pancreas	carcinoma	male	NA	NA	RPMI; 15% FBS; 20ug/ml human insulin
PANC1005_PANCREAS	CCLE	Pancreas	carcinoma	male	NA	primary	RPMI; 15% FBS; 2mM glutamine; 1.5 g/L Sodium bicarbonate; 4.5g/L glucose; 10mM HEPES; 1mM Sodium Pyruvate; 10 units/mL Insulin
PATU8988S_PANCREAS	CCLE	Pancreas	carcinoma	NA	NA	NA	"DMEM; 10%FBS, 2mMGlutamax"
PC14_LUNG	CCLE	Lung (NSCLC)	carcinoma	NA	NA	primary	RPMI; 10% FBS
PECAP34CLONEC12_UPPER_AERODIGESTIVE_TRACTE	CCLE	Upper Aerodigestive	carcinoma	male	60	primary	IMDM; 10% FBS; 2mM Glutamine
PF382_HAEMATOPOIETIC_AND_LYMPHOID_TISSUE	CCLE	T-cell ALL	lymphoid_neoplasm	NA	NA	NA	RPMI; 1640; 10%FBS
PK1_PANCREAS	CCLE	Pancreas	carcinoma	NA	NA	NA	RPMI; 10% FBS
PK45H_PANCREAS	CCLE	Pancreas	carcinoma	NA	NA	NA	RPMI; 10% FBS
PK59_PANCREAS	CCLE	Pancreas	carcinoma	NA	NA	NA	DMEM; 10% FBS
PLCPRF5_LIVER	CCLE	Liver	carcinoma	male	24	primary	RPMI; 10% FBS; 2mM glutamine
PSN1_PANCREAS	CCLE	Pancreas	carcinoma	NA	NA	primary	DMEM; 10% FBS
RCC10RGB_KIDNEY	CCLE	Kidney	carcinoma	male	NA	primary	RPMI; 10% FBS
RD_SOFT_TISSUE	CCLE	Soft Tissue	rhabdomyosarcoma	female	7	primary	"DMEM/HAM's F12 (1:1); 5% FBS; .005 mg/ml insulin, .01 mg/ml transferrin, 30nM sodium selenite, 10 nM hydrocortisone, 10 nM beta estradiol, 10 mM HEPES, 2 mM L-glutamine"
RERFLCAD1_LUNG	CCLE	Lung (NSCLC)	carcinoma	male	70	primary	RPMI; 10% FBS
RERFLCAL_LUNG	CCLE	Lung (NSCLC)	carcinoma	male	NA	primary	EMEM; 10% FBS
RH30_SOFT_TISSUE	CCLE	Soft Tissue	rhabdomyosarcoma	male	17	metastasis	RPMI; 10% FBS
RKN_SOFT_TISSUE	CCLE	Ovary	leionyosarcoma	female	45	primary	Hans F-12; 10% FBS
RKO_LARGE_INTESTINE	CCLE	Colorectal	carcinoma	NA	NA	primary	MEM; 10% FBS
RMUGS_OVARY	CCLE	Ovary	carcinoma	female	62	primary	Hans F-12; 10% FBS
RPMI7951_SKIN	CCLE	Melanoma	malignant_melanoma	female	18	metastasis	RPMI; 10% FBS
RT112_URINARY_TRACT	CCLE	Urinary Tract	carcinoma	female	NA	primary	RPMI; 10% FBS
RT11284_URINARY_TRACT	CCLE	Urinary Tract	carcinoma	NA	NA	NA	EMEM; 10% FBS;2mMGlutamax; 1%NEAA
RT4_URINARY_TRACT	CCLE	Melanoma	malignant_melanoma	male	NA	NA	M10
RVH421_SKIN	CCLE						RPMI; 10% FBS

Name	Source	Lineage	Histology	Gender	Age	Primary/Metastasis	Achilles culture medium
SCABER_URINARY_TRACT	CCLE	Urinary Tract	carcinoma	NA	NA	NA	"E10+ L-glutamine: 2.0 mM, NEAA( Non-essential Amino Acids): 0.1 mM, Sodium Pyruvate: 0.1 mM"
SF295_CENTRAL_NERVOUS_SYSTEM	CCLE	Glioma	glioma	female	67	primary	RPMI; 10% FBS
SF767_CENTRAL_NERVOUS_SYSTEM	"Lynda Chin, MD Anderson"	Glioma	glioma	female	NA	NA	DIMEM; 10% FBS
SH10TC_STOMACH	CCLE	Stomach	carcinoma	NA	NA	NA	RPMI; 10% FBS
SIMA_AUTONOMIC_GANGLIA	CCLE	Neuroblastoma	neuroblastoma	male	NA	NA	RPMI; 10% FBS
SJSA1_BONE	CCLE	Osteosarcoma	osteosarcoma	male	19	primary	RPMI; 10% FBS
SKBR3_BREAST	CCLE	Breast	carcinoma	female	43	metastasis	McCoy's 5A; 10% FBS
SKHEP1_LIVER	CCLE	Liver	carcinoma	male	52	metastasis	EMEM; 10% FBS
SKMEL24_SKIN	CCLE	Melanoma	malignant_melanoma	male	67	metastasis	EMEM; 10% FBS
SKMEL30_SKIN	CCLE	Melanoma	malignant_melanoma	male	67	metastasis	RPMI; 10% FBS
SKMES1_LUNG	CCLE	Lung (NSCLC)	carcinoma	male	65	metastasis	DIMEM; 10% FBS
SKNAS_AUTONOMIC_GANGLIA	CCLE	Neuroblastoma	neuroblastoma	female	NA	NA	DIMEM; 10% FBS; NEAA
SKNB22_AUTONOMIC_GANGLIA	CCLE	Neuroblastoma	neuroblastoma	male	NA	NA	EMEM/F12 (1:1); 10% FBS
SKNDZ_AUTONOMIC_GANGLIA	CCLE	Neuroblastoma	neuroblastoma	female	NA	NA	DIMEM; 10% FBS; NEAA
SKNFL_AUTONOMIC_GANGLIA	CCLE	Neuroblastoma	neuroblastoma	male	NA	NA	DIMEM; 10% FBS; NEAA
SKNMC_BONE	CCLE	Ewing Sarcoma	Ewings_sarcoma-peripheral_primitive_neuroectodermal_tumor	female	NA	NA	EMEM; 10% FBS
SKOV3_OVARY	CCLE	Ovary	carcinoma	female	64	metastasis	McCoy's 5A; 10% FBS
SLR20_KIDNEY	"Kaelin Lab, DFCI"	Kidney	carcinoma	NA	NA	primary	RPMI; 10% FBS
SLR23_KIDNEY	"Kaelin Lab, DFCI"	Kidney	carcinoma	NA	NA	primary	RPMI; 10% FBS
SLR26_KIDNEY	"Kaelin Lab, DFCI"	Kidney	carcinoma	NA	NA	primary	RPMI; 10% FBS
SNGM_ENDOMETRIUM	CCLE	Endometrium	carcinoma	NA	NA	NA	Ham F-12: 80.0%
SNUL_STOMACH	CCLE	Stomach	carcinoma	NA	NA	NA	RPMI-1640: 90.0%
SNU201_CENTRAL_NERVOUS_SYSTEM	CCLE	Glioma	glioma	male	58	primary	RPMI; 10% FBS
SNU213_PANCREAS	CCLE	Pancreas	carcinoma	male	NA	NA	"RPMI; 10% FBS, 2mM L-glutamine"
SNU349_KIDNEY	CCLE	Kidney	carcinoma	male	68	primary	RPMI; 10% FBS
SNU398_LIVER	CCLE	Liver	carcinoma	NA	NA	NA	RPMI; 10% FBS
SNU410_PANCREAS	CCLE	Pancreas	carcinoma	male	NA	NA	RPMI; 10% FBS
SNU449_LIVER	CCLE	Liver	carcinoma	NA	NA	NA	RPMI; 10% FBS
SNU503_LARGE_INTESTINE	CCLE	Colorectal	carcinoma	male	NA	NA	RPMI; 10% FBS
SNU685_ENDOMETRIUM	CCLE	Endometrium	carcinoma	female	NA	NA	RPMI; 10% FBS

Name	Source	Lineage	Histology	Gender	Age	Primary/Metastasis	Achilles culture medium
SNU8_OVARY	CCLE	Ovary	carcinoma	female	55	primary	RPMI; 10% FBS
SNU840_OVARY	CCLE	Ovary	carcinoma	female	45	primary	RPMI; 10% FBS
SUIT2_PANCREAS	CCLE	Pancreas	carcinoma	NA	NA	NA	RPMI; 10% FBS
SUPM2_HAEMATOPOIETIC_AND_LYMPHOID_TISSUE	CCLE	Lymphoma (ALCL)	lymphoid_neoplasm	female	NA	NA	RPMI; 20% FBS
SUPT1_HAEMATOPOIETIC_AND_LYMPHOID_TISSUE	CCLE	T-cell ALL	lymphoid_neoplasm	male	8	metastasis	RPMI; 10% FBS
SW1463_LARGE_INTESTINE	CCLE	Colorectal	carcinoma	female	NA	NA	Leibovitz's L-15; 10%FBS
SW403_LARGE_INTESTINE	CCLE	Colorectal	carcinoma	female	51	primary	RPMI; 10% FBS
SW48_LARGE_INTESTINE	CCLE	Colorectal	carcinoma	female	82	primary	RPMI; 10% FBS
SW620_LARGE_INTESTINE	CCLE	Colorectal	carcinoma	male	51	metastasis	L-15; 10% FBS
SW837_LARGE_INTESTINE	CCLE	Colorectal	carcinoma	male	53	primary	RPMI; 10% FBS
T24_URINARY_TRACT	CCLE	Urinary Tract	carcinoma	NA	NA	NA	McCoy 5A; 90.0%
T3M4_PANCREAS	CCLE	Pancreas	carcinoma	NA	NA	NA	Ham F-10; 90.0%;10%FBS
T84_LARGE_INTESTINE	CCLE	Colorectal	carcinoma	male	NA	NA	DMEM:FL12(1); 5% FBS; 2mM Glutamine
T98G_CENTRAL_NERVOUS_SYSTEM	CCLE	Glioma	glioma	male	61	primary	EMEM; 10% FBS
TCCPAN2_PANCREAS	CCLE	Pancreas	carcinoma	female	NA	NA	RPMI; 10% FBS
TCCSUP URINARY TRACT	CCLE	Urinary Tract	carcinoma	female	67	primary	EMEM; 10% FBS; 1mM NEAA; 1mM Sodium Pyruvate
TE1_OESOPHAGUS	CCLE	Esophagus	carcinoma	male	NA	NA	RPMI; 10% FBS
TE5_OESOPHAGUS	CCLE	Esophagus	carcinoma	NA	NA	NA	RPMI; 10% FBS
TEN_ENDOMETRIUM	CCLE	Endometrium	carcinoma	NA	NA	NA	MEM;10%FBS
TF1_HAEMATOPOIETIC_AND_LYMPHOID_TISSUE	CCLE	AML	haematopoietic_neoplasm	male	NA	NA	RPMI-1640; 10%FBS; 2ng/ml GM-CSF
THP1_HAEMATOPOIETIC_AND_LYMPHOID_TISSUE	CCLE	AML	haematopoietic_neoplasm	male	1	primary	RPMI; 10% FBS; 50μM B-mercaptoethanol
TOV21G_OVARY	CCLE	Ovary	carcinoma	female	62	primary	MCDB 105:Medium 199 (1:); 15% FBS
TUHR10TKB_KIDNEY	CCLE	Kidney	carcinoma	NA	NA	primary	RPMI; 10% FBS
TUHR4TKB_KIDNEY	CCLE	Kidney	carcinoma	NA	NA	primary	DMEM; 10% FBS
U118MG_CENTRAL_NERVOUS_SYSTEM	CCLE	Glioma	glioma	male	NA	primary	DMEM; 10% FBS
U178_CENTRAL_NERVOUS_SYSTEM	CCLE	Glioma	glioma	male	NA	primary	DMEM; 10% FBS
U251MG_CENTRAL_NERVOUS_SYSTEM	CCLE	Osteosarcoma	osteosarcoma	female	15	primary	McCoy's 5A; 10% FBS
U2OS_BONE	CCLE	"Lynda Chin, MD Anderson"	glioma	NA	NA	NA	DMEM; 10% FBS
U343_CENTRAL_NERVOUS_SYSTEM	CCLE	Glioma	glioma	female	44	primary	EMEM; 10% FBS
U87MG_CENTRAL_NERVOUS_SYSTEM	CCLE	Glioma	glioma	male	37	metastasis	RPMI; 10% FBS
U937_HAEMATOPOIETIC_AND_LYMPHOID_TISSUE	CCLE	Lymphoma (DLBCL)	lymphoid_neoplasm				

Name	Source	Lineage	Histology	Gender	Age	Primary/Metastasis	Achilles culture medium
UACC257_SKIN	CCLE	Melanoma	malignant_melanoma	NA	NA	primary	RPMI; 10% FBS
UACC62_SKIN	CCLE	Melanoma	malignant_melanoma	NA	NA	NA	RPMI; 10% FBS
UMUC3_URINARY_TRACT	CCLE	Urinary Tract	carcinoma	NA	NA	NA	EMEM; 10% FBS
UOK101_KIDNEY	"Kaelin Lab, DFCI"	Kidney	carcinoma	female	NA	NA	DMEM; 10% FBS
VMCUB1_URINARY_TRACT	CCLE	Urinary Tract	carcinoma	NA	NA	NA	DMEM; 10% FBS
WM115_SKIN	CCLE	Melanoma	malignant_melanoma	female	NA	NA	EMEM; 10% FBS
WM1799_SKIN	CCLE	Melanoma	malignant_melanoma	NA	NA	NA	RPMI; 10% FBS
WM2664_SKIN	CCLE	Melanoma	malignant_melanoma	female	NA	NA	DMEM; 10% FBS
WM793_SKIN	CCLE	Melanoma	malignant_melanoma	NA	NA	NA	RPMI; 10% FBS
WM983B_SKIN	CCLE	Melanoma	malignant_melanoma	NA	NA	NA	RPMI; 10% FBS
YAPC_PANCREAS	CCLE	Pancreas	carcinoma	male	NA	NA	RPMI; 10% FBS
YKG1_CENTRAL_NERVOUS_SYSTEM	CCLE	Glioma	glioma	female	NA	primary	DMEM; 10% FBS
ZR751_BREAST	CCLE	Breast	carcinoma	female	NA	NA	RPMI; 10% FBS